Regulation of Stress-Inducible Phosphoprotein 1 Nuclear Retention by Protein Inhibitor of Activated STAT PIAS1

Iaci N. Soares‡§‖[f], Fabiana A. Caetano‡§‖[f], Jordan Pinder, Bruna Roz Rodrigues‡‡, Flavio H. Beraldo‡¶, Valeriy G. Ostapchenko‡¶, Chantal Durette§§, Grace Schenatto Pereira¶¶, Marilene H. Lopes‖‖, Nicolle Queiroz-Hazarbassanov‡‡, Isabela W. Cunha[a], Paulo I. Sanematsu[b], Sergio Suzuki[b], Luiz F. Bleggi-Torres[c], Caroline Schild-Poulter‡[d], Pierre Thibault§§, Graham Dellaire**, Vilma R. Martins‡‡[e], Vania F. Prado‡§¶[e], and Marco A. M. Prado‡§¶[e]**

Stress-inducible phosphoprotein 1 (STI1), a cochaperone for Hsp90, has been shown to regulate multiple pathways in astrocytes, but its contributions to cellular stress responses are not fully understood. We show that in response to irradiation-mediated DNA damage stress STI1 accumulates in the nucleus of astrocytes. Also, STI1 haploinsufficiency decreases astrocyte survival after irradiation. Using yeast two-hybrid screenings we identified several nuclear proteins as STI1 interactors. Overexpression of one of these interactors, PIAS1, seems to be specifically involved in STI1 nuclear retention and in directing STI1 and Hsp90 to specific sub-nuclear regions. PIAS1 and STI1 co-immunoprecipitate and PIAS1 can function as an E3 SUMO ligase for STI. Using mass spectrometry we identified five SUMOylation sites in STI1. A STI1 mutant lacking these five sites is not SUMOylated, but still accumulates in the nucleus in response to increased expression of PIAS1, suggesting the possibility that a direct interaction with PIAS1 could be responsible for STI1 nuclear retention. To test this possibility, we mapped the interaction sites between PIAS1 and STI1 using yeast-two hybrid assays and surface plasmon resonance and found that a large domain in the N-terminal region of STI1 interacts with high affinity with amino acids 450–480 of PIAS1. Knockdown of PIAS1 in astrocytes impairs the accumulation of nuclear STI1 in response to irradiation. Moreover, a PIAS1 mutant lacking the STI1 binding site is unable to increase STI1 nuclear retention. Interestingly, in human glioblastoma multiforme PIAS1 expression is increased and we found a significant correlation between increased PIAS1 expression and STI1 nuclear localization. These experiments provide evidence that direct interaction between STI1 and PIAS1 is involved in the accumulation of nuclear STI1. This retention mechanism could facilitate nuclear chaperone activity. ***Molecular & Cellular Proteomics 12: 10.1074/mcp.M113.031005, 3253–3270, 2013.***

Stress-inducible phosphoprotein I (STI1)[1] is a conserved cochaperone protein that assists Hsp90 in managing client proteins, by mediating the transfer of proteins between Hsp70

From the ‡Robarts Research Institute, The University of Western Ontario, London, ON, Canada; §Department of Anatomy and Cell Biology, University Western Ontario, London, ON, Canada; ¶Department of Physiology and Pharmacology, University Western Ontario, London, ON, Canada; ‖Program in Molecular Medicine, Universidade Federal de Minas Gerais, Brazil; **Department of Pathology, Dalhousie University, Halifax, Nova Scotia, Canada; ‡‡International Research Center, A. C. Camargo Cancer Center, National Institute for Translational Neuroscience and National Institute for Oncogenomics (CNPq/MCT), São Paulo, Brazil; §§Institute for Research in Immunology and Cancer, Université de Montréal, Montréal, QC, Canada; ¶¶Department of Physiology and Biophysics – Universidade Federal de Minas Gerais, Belo Horizonte, MG, Brazil; ‖‖Department of Cell and Developmental Biology, Universidade de Sao Paulo and National Institute for Translational Neuroscience, Sao Paulo, SP, Brazil; [a]Departament of Pathology, AC Camargo Cancer Center, São Paulo, Brazil; [b]Department of Neurosurgery, AC Camargo Cancer Center, São Paulo, Brazil; [c]Department of Pathology, Universidade Federal do Paraná, Curitiba, Brazil and Pelé Pequeno Príncipe Research Institute, Curitiba, Brazil; [d]Department of Biochemistry, University of Western Ontario, London, ON, Canada

Received May 21, 2013, and in revised form, July 15, 2013
Published, MCP Papers in Press, August 12, 2013, DOI 10.1074/mcp.M113.031005

[1] The abbreviations used are: STI1, stress inducible phosphoprotein 1; ACVS, Animal Care and Veterinarian Service; ATM, ataxia telangiectasia mutated; CCAC, Canadian Council of Animal care; CNS, central nervous system; DDR, DNA damage response; DSB, double strand break; PIAS, protein inhibitor of activated STAT; GBM, glioblastoma multiforme; Hsp70, heat shock protein 70; Hsp90, heat shock protein 90; IHC, immunohistochemistry; IR, ionizing radiation; LDH, lactate dehydrogenase; NHEJ, nonhomologous end-joining; NEM, N-ethylmaleimide; Pc2, polycomb protein 2; PML – NB, promyelocytic leukemia nuclear bodies; ROI, region of interest; SD, synthetic dropout; SEM, standard error of mean; SIM, SUMO-interacting motif; siRNA, small interference RNA; STAT, Signal Transducer and Activator of Transcription; SUMO, small ubiquitin-like modifier; SPR, surface plasmon resonance; TFA, trifluoroacetic acid; TMA, tissue microarrays; TPR, tetratricopeptide repeat domains; UBC9, ubiquitin conjugating enzyme.

and Hsp90 (1–3). STI1 contains several tetratricopeptide-repeat domains (TRP) that can serve as interaction modules with Hsp90 and Hsp70 (4). STI1 helps to drive the sequential steps involved in the Hsp90 chaperone machinery (5) and regulates the ATPase activity of Hsp90 (6, 7). STI1 is also secreted by distinct cells (8–12), using a noncanonical mechanism involving extracellular vesicles (11). Secreted STI1 can activate multiple signaling pathways in distinct cell types (8–10, 13–18).

Elimination of STI1 in yeast sensitizes cells to Hsp90 inhibitors, but it is not by itself lethal (19). STI1 can also be eliminated in *C. elegans*, although it results in decreased life span (20). In contrast, STI1 mutant mice do not survive E10.5 and present several morphological defects, owing to decreased levels of several Hsp90-client proteins (21). Mouse embryonic fibroblasts obtained from STI1-deficient embryos also fail to thrive and present increased levels of the DNA damage marker γ-H2AX, suggestive of increased cellular stress (21). Hence, in mammals STI1 seems to play additional roles in cellular survival that are not yet fully understood.

STI1 is abundantly expressed in the cytoplasm of cells, but can also be found in the Golgi (22), in vesicles and in multivesicular bodies (11). Moreover, this cochaperone has been shown to shuttle between the cytoplasm and the nucleus in cell lines (23). Cellular stress, arrest in G1/S phase of the cell cycle and phosphorylation are factors that seem to regulate STI1 nuclear localization (23, 24). Presumably nuclear STI1 can regulate chaperone activity, but whether it can interact with nuclear proteins is unknown.

Previous experiments using cell lines have shown that knockdown of STI1 increases susceptibility of cells to irradiation (25). Whether changes in STI1 levels in primary differentiated cells, such as astrocytes, may affect their response to irradiation stress is unknown. This is of interest, as astrocytes, which can give rise to distinct tumor cells, are highly radioresistant (26). Indeed, astrocytes have a noncanonical DNA damage response (DDR) to irradiation (26). Here we show that STI1 undergoes nuclear translocation in astrocytes after γ-radiation-induced DNA damage. Moreover, astrocytes haploinsufficient for STI1 are more susceptible to cell death induced by irradiation. To understand potential mechanisms involved with STI1 nuclear retention, we have performed yeast-two hybrid screenings to identify STI1 nuclear partners. We identified protein inhibitor of activated STAT (PIAS1) as a direct interactor of STI1 and provide evidence that it acts as a small ubiquitin-like modifier (SUMO) E3 ligase for STI1. We show this interaction is involved with STI1 nuclear retention after irradiation. Interestingly, tissue microarray analysis demonstrated that higher PIAS1 levels are found in glioblastoma multiforme (GBM) when compared with non-neoplastic tissue. Furthermore, we uncovered a positive relationship between increased PIAS1 expression in GBMs and augmented STI1 nuclear localization. Our results reveal a novel mechanism by which increased expression of PIAS1, as observed in GBM, can increase the retention of nuclear STI1, a critical regulator of the chaperone machinery.

EXPERIMENTAL PROCEDURES

Plasmids—YFP-Ubc9 and FLAG-Pc2 were kindly provided by Dr. David Wotton (Professor of Biochemistry and Molecular Genetics of University of Virginia, Charlottesville, US). The plasmids Myc-PIAS4 and Myc-PIAS1 were kindly provided by Dr. Lienhard Schmitz (Institute of Biochemistry, Medical Faculty Friedrichstrasse, Justus-Liebig University, Giessen, Germany). GFP-STI1 and YFP-STI1 were generated by cloning STI1 in the SalI and KpnI restriction sites, and XhoI and KpnI restriction sites of pEGFP-C1 and pEYFP-N1, respectively (Clontech, Mountain View, CA). PML-YFP was kindly provided by Marc Tini (Department of Physiology and Pharmacology, Schulich School of Medicine and Dentistry, University of Western Ontario). HA-STI1 was constructed by cloning STI1 in pCMVHA (Clontech) using the restriction enzymes SalI and SfiI (BioLabs). Mutants of STI1 were generated in the pCMVHA construct. A mouse N-terminal (bp 1–870) portion of STI1, or smaller fragments within this region, were amplified and ligated in frame with the yeast Gal4 DNA-binding domain ($Gal4_{DBD}$) in the vector pGBKT7 (BD Biosciences, pGBKT7-N-STI1). Full-length and truncated PIAS1 sequences were cloned into pACT2 (Clontech) in frame with the yeast Gal4 transcriptional activation domain ($Gal4_{AD}$). Site-directed mutagensis of PIAS1 was performed by overlap extension PCR.

Mouse Line Generation—Genetically modified mice were generated using standard homologous recombination techniques, using C57BL/6j ES cells. Mice were generated by Ozgene (Australia). Chimeric mice were bred to C57BL/6j mice and germline transmission of the mutant STI1 allele was identified by Southern blot (not shown). F1 mice were crossed to constitutively expressing Cre mice to remove loxP flanked regions. Cre recombined mice were then crossed to C57BL/6j mice and progeny bearing the recombined STI1 allele, but lacking the Cre transgene, were identified by Southern analysis (not shown). These mice were then used to expand the colony. $STI1^{-/+}$ mice were then intercrossed to generate $STI1^{-/-}$ mice. These mice presented early embryonic lethality (E10.5) and a range of developmental defects (21). We have attempted to generate mice with a conditional STI1 floxed allele, however we found that after removal of the Neo-cassete this particular floxed allele was null and also caused embryonic lethality (results not shown). Hence, astrocytes could be isolated only from $STI1^{-/+}$ mice. Haploinsufficient astrocytes have no difference in their cell cycle and proliferative properties compared with wild-type astrocytes (21).

Primary Culture of Astrocytes—Animals were maintained and handled in the mouse vivarium at University of Western Ontario Animal Care and Veterinarian Service (ACVS). Procedures were conducted in accordance with the animal care guidelines of the CCAC. This study was approved by the AUS committee at the University of Western Ontario (Protocol # 2008–127). Nineteen day time-pregnant mice (C57BL6/j) were euthanized and embryos were quickly removed and decapitated to isolate cortical astrocytes (10). Cortical hemispheres were dissected and separated from the striatum. Cortices were dissociated in 5 ml Dulbecco's modified Eagle's medium supplemented with 10% (v/v) fetal bovine serum and 1% (v/v) penicillin/streptomycin by pipetting up and down several times with a serological pipette and plated with additional 5 ml of medium in a 100 mm Petri dish. Cultures were maintained in incubator at 37 °C, 5% CO_2. Astrocytes were used after 10–11 days *in vitro*.

Cell Culture, Transfections and Co-Immunoprecipitation—CF-10 cells were cultured and transfected as previously described (13). HEK293 cells were grown and transfected as described (14). Fourth-eight hours after transfection, cells were suspended in 300 μl of lysis buffer containing 50 mM Tris-HCl,150 mM NaCl pH 7.5, with 0.5% or

1% Triton X-100, 20 mM N-ethylmaleimide (NEM) and Protease Inhibitor Mixture (Sigma). A total of 800–900 μg of protein extract were incubated with 50 μl of anti-HA agarose-conjugated beads (Sigma); subsequent steps followed the manufacturer's protocols. Cell lines were usually transfected with 80% efficiency. Astrocytes were transfected with 30–40% efficiency.

Western-Blot—Cell extracts were prepared according to the methodologies described above. Protocols for the Western blots were previously described (14, 27). The antibodies used were: anti-FLAG (Sigma, 1:1000); anti-Ubc9 (Invitrogen, Carlsbad, CA; 1:1000); anti-MYC (1:1000), and anti-HA (1:1000) from Abcam (Cambridge, MA); anti-PIAS1 (Santa Cruz, Santa Cruz, CA; 1:500, or Abcam, 1:1000); anti-PIAS4 (Santa Cruz, 1:500); anti-STI1 (1:5000) (28). All blots were quantified using the imaging system FluorChem® Xplor (Alpha Innotech) and Image J software.

Immunofluorescence—For detection of endogenous or overexpressed proteins, cotransfected CF10 cells or astrocytes were fixed in 4% paraformaldehyde (Polyscience, Warrington, PA) for 20 min at room temperature and immunostained as described (29). Primary antibody used were Anti-Myc (Abcam, 1:100), for detection of PIAS1 or PIAS4-Myc; anti-Flag (Sigma, 1:100), for detection of Pc2; anti-Histone H2A.X S139 (Cell Signaling, Danvers, MA; 1:100), for detection of foci formation; anti-STI1 (1:200) and anti-Hsp90 (Abcam, 1:50), for detection of endogenous STI1 and Hsp90 respectively.

Fluorescence Imaging—Confocal microscopy was performed using a Bio-Rad MRC 1024 laser scanning confocal system running the Lasersharp 3.0 software coupled to a Zeiss microscope (Axiovert 100) with a 100×/1.4 or 63×/1.3 oil-immersion lens (Zeiss); a LSM 510 Meta laser-scanning confocal system coupled to a Zeiss microscope or a Leica SP5 laser-scanning confocal microscope using a 63×/1.2 water-immersion or a 63x/1.4 oil-immersion lens (Leica). Image analysis and processing were performed with Lasersharp (Bio-Rad), Confocal Assistant, Adobe Photoshop, Metamorph, Leica Application Suite Advanced Fluorescent Lite, and ImageJ (version 1.24) software.

Irradiation and Nuclear STI1 and Foci Counting—Cells were plated, transfected with constructs of interest and after 48 h the dishes were placed in a Faxitron RX-650 to receive a dose rate of 2 Gy/min. Cells were lysed or fixed for different periods of time after irradiation. Ten random fields of each dish were imaged and then analyzed by number of cells, number of cells with nuclear STI1 (defined as homogenous labeling in the cells, compared with nonirradiated cells that present no staining in the nucleus for STI1) and total number of foci. The results were then normalized by the total number of cells, which was >200 for each experiment.

Live/Dead Assay—STI1$^{-/+}$ and STI1$^{+/+}$ astrocytes were plated in glass-bottom culture dishes (MatTek, Ashland, MA) irradiated and used 48 h later. Subsequent steps were performed according to the Live/Dead Assay Kit (Invitrogen). Ten random fields were imaged per dish and live or dead cells were then counted with the cell counting tool from Image J software.

LDH Release Assay—STI1$^{-/+}$ and STI1$^{+/+}$ astrocytes were counted and 2×10^5 cells were plated on 35-mm Petri dishes. Dishes were irradiated for 10 min at 2 Gy and 48 h later 50% of their medium were collected and cleared from debris by centrifuging. Subsequent steps were done following the manufacturer's protocols (LDH assay Sigma kit #MAK066–1KT).

Yeast Two-Hybrid Screening—Yeast strain AH109 was transformed with pGBKT7 (Empty vector) or pGBKT7- N-STI1 and transformants were selected on S.D. (synthetic dropout) plates, in which the media lacks Trp. These selected yeast cells were transformed with a mouse brain cDNA library (title 4.2×10^7 cfu/ml) fused with Gal4ad in the vector pACT2 (Leu) (Clontech). 1.0×10^6 independent clones were screened and yeast cells were selected for growth on Ade/His/Leu/Trp - deficient medium and tested for *lacZ* expression according to instructions provided by the manufacturer (Clontech). The same STI1 construct was used for another screening using the yeast mating protocol with a BD Matchmaker™ pretransformed human brain cDNA library (title 1.3×10^8 cfu/ml) fused with Gal4ad in the vector pACT2. Procedures were carried out according to manufacturer's protocols (Clontech). The Matting efficiency was 9.4% and 3.9×10^7 clones were screened. Attempts to express a C-terminal STI1 construct is yeast did not work, so we restricted our analysis to the N terminus.

Yeast two-hybrid assays for mapping the interaction domains of PIAS1 and STI1 were carried out using diploid yeast cotransformants produced by mating yeast strains Y187 and Y2HGold (Clontech) transformed with pACT2- and pGBKT7-based plasmids, respectively.

Surface Plasmon Resonance—Surface plasmon resonance was studied using Biacore X system (GE Healthcare, Pittsburgh, PA) equipped with a CM5 chip. Recombinant STI1 and PIAS1 peptides were produced using pE-SUMOstar Amp Kit (LifeSensors, Malvern, PA) and purified to >95% purity estimated by SDS-PAGE. STI1 was covalently bound to the chip using standard amine-coupling NHS/EDC procedure (30) to the level of ~8000 response units (RU). Before injections the chip was equilibrated in the running buffer (25 mM HEPES, 150 mM NaCl, pH 8.0). Different concentrations of PIAS1 peptides in the running buffer were injected at 5 μl/min rate for 6 min. After that 2-min "off" reactions were recorded followed by washing with running buffer. Between injections the chip was additionally washed at 100 μl/min with 1-min injections of 10 mM HCl. The background signal was obtained by injecting the same peptides through a control flow cell with no bound STI1. Binding curves were analyzed with Biacore software and GraphPad Prism 5 (GraphPad Software, San Diego, CA). "On" curves were fitted with a one-site interaction model. Off curves were fitted with an exponential decay model.

In Vitro SUMOylation—Reactions were prepared with 1 μg of SUMO-activating enzyme 1 (Aos1/Uba2) (human recombinant), 4 μg of untagged ubiquitin conjugating enzyme UBC9 (SUMO E2) (human, recombinant), 4 μg of His6-tagged SUMO proteins 1, 2, or 3, (human recombinant) in SUMOylation Buffer plus 0.01 M Mg-ATP. All reagents were obtained from a SUMOylation kit (BIOMOL International, Farminfdale, NY). Either 1 μg of His tagged STI1 (mouse recombinant) or 4 μg of GST-tagged RanGAP1 (positive control, human recombinant) were tested according to the kit manufacturer's protocols.

Identification of SUMOylation Sites by Mass Spectrometry—For *in vitro* STI1 SUMOylation, 10 μg of His tagged STI1 (mouse), 3 μg of SUMO-activating enzyme 1 (Aos1/Uba2) (human recombinant), 25 μg of untagged Ubiquitin Conjugating Enzyme UBC9 (SUMO E2) (human), 10 μg of His6-tagged SUMO3 mutant protein (human) were added to SUMOylation Buffer containing 0.6 M Mg-ATP. This mixture was incubated at 37 °C under agitation for 1.5 h. 8 M urea was then added to the final concentration of 4 M. Proteins were reduced with 5 mM tris-(2-carboxyethyl)-phosphine (TCEP, Pierce) for 20 min at 37 °C and then alkylated with 50 mM chloroacetamide (Sigma-Aldrich) for 20 min at 37 °C. Excess chloroacetamide was neutralized by addition of 50 mM dithiothreitol. The solution was diluted to 1 M urea with 50 mM ammonium bicarbonate and digested overnight with modified trypsin (1:50, enzyme:substrate ratio) at 37 °C with high agitation. The digest was acidified with trifluoroacetic acid (TFA), desalted using an Oasis HLB cartridge (Waters, Milford, MA) and dried in a speed vacuum concentrator.

LC-MS/MS analyses were performed on a nano-LC 2D pump (Eksigent) coupled to a LTQ-Orbitrap Velos mass spectrometer via a nanoelectrospray ion source (Thermo Fisher Scientific). Peptides were loaded on an Optiguard SCX trap column (5 μm particle, 300Å, 0.5 ID × 23 mm, Optimize Technologies) and eluted on a 360 μm ID × 4 mm, C_{18} trap column before separation on a custom-made 150 μm

ID × 10 cm nano-LC column (Jupiter C_{18}, 3 μm, 300 Å, Phenomenex). Tryptic digests were loaded on the SCX trap and sequentially eluted using salt plugs of 0, 250, 500, 750 mM, 1, and 2 M ammonium acetate, pH 3.5. Peptides were separated on the analytical column using a linear gradient of 5–40% acetonitrile (0.2% formic acid) in 53 min with a flow rate of 600 nL/min. The mass spectrometer was operated in data dependent mode to automatically switch between survey MS and MS/MS acquisitions. The conventional MS spectra (survey scan) were acquired in the Orbitrap at a resolution of 60,000 for *m/z* 400 after accumulation of 10^6 ions in the linear ion trap. Mass calibration used a lock mass from ambient air [protonated $(Si(CH_3)_2O))_6$; *m/z* 445.120029], and provided mass accuracy within 5 ppm for precursor and fragment ion mass measurements. MS/MS spectra were acquired in HCD activation mode using an isolation window of 2 Da. Precursor ions were accumulated to a target value of 30,000 with a maximum injection time of 100 ms and fragment ions were transferred to the Orbitrap analyzer operating at a resolution of 15,000 at *m/z* 400. The dynamic exclusion of previously acquired precursor ions was enabled (repeat count 1, repeat duration: 30 s; exclusion duration 45 s).

MS data were acquired using the Xcalibur software (version 2.1 build1139). Peak lists were generated using Mascot distiller (version 2.3.2.0, Matrix science) and MS/MS spectra were searched against the IPI human database containing 75429 forward sequences (version 3.54, released Jan 2009) using Mascot (version 2.3.2, Matrix Science) with a mass tolerance of 10 ppm for precursor ions and 0.05 Da for fragments. The number of allowed missed cleavage sites for trypsin was set to 3 and oxidation (M), deamidation (NQ), carbamidomethylation (C) and SUMOylation (K) (GGTQN: SUMO3) were selected as variable modifications. A software application was developed to search mascot generic files (mgf) for specific SUMO3 fragment ions (*e.g. m/z* 132.0768, 226.0822, 243.1088, 344.1565, 401.1779; and neutral losses of SUMO3 remnant) to produce a mgf file containing only MS/MS spectra of potential SUMOylated peptide candidates. SUMO fragment ions were removed from the corresponding mgf files and searched again using Mascot as indicated above. Manual inspection of all MS/MS spectra for modified peptides was performed to validate assignments.

Mutations—About 50–100 ng of pCMV5-HA STI1 were used to generate point mutations or deletion mutants. Primers were designed using Stratagene Software tool for QuikChange® Multi Site-Directed Mutagenesis Kit. PCR mix, cycle parameters and transformation in competent cells were done following the kit manufacturer's protocols. Sequence of primers is available on request. All mutants were confirmed by sequencing.

Quantification of Fluorescence—Intracellular distribution of STI1 was evaluated using the MetaMorph software. Total fluorescence in the nucleus was measured and normalized by the total of fluorescence of the cytoplasm. The area of each cell was considered during analyzes. Regions of interest were determined and total fluorescence was detected automatically and independently by the software. Results were expressed as the mean of total fluorescence in the nucleus/cytosol per cell. Colocalization analysis was evaluated using Image J software. Each image first had its channels split; cells nuclei were the chosen region of interest (ROI) and backgrounds were subtracted before colocalization measurement. The software detects the pixels that colocalize between the channels and calculates the Manders M coefficient for each image, which identifies the percentage of pixels on one channel overlapping with the other.

siRNA Transfection—A total of 0.8 μg of PIAS1 siRNA (NM_016166) (Qiagen) and fluorescent nonrelevant siRNA controls (Invitrogen) were used to transfect astrocytes with the Effectene transfection kit (QUIAGEN). For these experiments cells were incubated with the reagents for 24 h and used 72 h after transfection.

Patients and Tissue Microarrays—Tissue microarrays (TMA) were prepared from formalin-fixed, paraffin-embedded GBMs (from Department of Pathology of AC Camargo Cancer Center) and 14 non-neoplasic samples (from surgically remediable patients with intractable mesial temporal lobe epilepsy from the Department of Pathology, Federal University of Parana, Brazil). Samples were prepared after approval from AC Camargo Cancer Center Research and Ethics Committee (Process 1613/11 and 1692/12). From May 1980 to December 2004, 91 patients with GBMs underwent surgical treatment at the Neurosurgery Department of AC Camargo Cancer Center. Analysis of PIAS1 and STI1 expression was possible in 87 cases (60% males; mean age 53.5 ± 18.3 y). None of these patients were treated before surgery.

For immunohistochemistry (IHC), TMAs were incubated overnight with primary antibody anti-PIAS1 (1:40, Cell Signaling) or anti-STI1 (1:40, Stressgen Bioreagents, AnnArbor, MI) at 4 °C, after antigen retrieval. TMAs were incubated for 60 min at 37 °C with EnVision labeled polymer peroxidase (Dako), developed using 3,3-diaminobenzidine tetrahydrochloride (Sigma), and counterstained with hematoxylin. Sections were observed under an Olympus IMT2-NIC microscope. Virtual slides were created with the ScanScope System (Aperio Technologies). The percentage of positive PIAS1 and STI1 nuclei was calculated according to the internal algorithm with ImageScope (IHC Nuclear v1).

Statistical Analysis—Mean values of at least three independent datasets are shown in the figures; the error bars represent S.E. Student's *t* test was used to compare two groups. ANOVA followed by appropriate post-hoc tests was used for multiple comparisons. PIAS1 expression and STI1 nuclear localization in samples from patients with gliblastomas were correlated using Pearson's correlation coefficient. For all tests, results were considered statistically significant when p value was < 0.05.

RESULTS

STI1 Accumulates in the Nucleus of Astrocytes in Response to γ-Radiation—Previous experiments have shown that increased cellular stress by heat shock, or treatment with hydroxiurea, which arrests cell cycle, causes nuclear retention of STI1 in cell lines (23, 24). To test the possibility that STI1 participates in the response to genotoxic stress in astrocytes, we used ionizing radiation (IR, 2Gy/10min). To monitor DNA damage in response to IR we measured phosphorylated histone H2AX (γ-H2AX S139), a well-established marker of double-strand breaks (DSBs) and accumulation of nuclear foci (31), as this is the most suitable marker for DNA damage in astrocytes (26). We found that IR led to fast recruitment of STI1-YFP (Fig. 1*A*) or endogenous STI1 to the nucleus (Fig. 1B), detected as increased proportion of astrocytes presenting nuclear STI1 labeling (Fig. 1C). This increased nuclear localization of STI1 persisted up to 24 h after IR treatment. Concomitant increase of γ-H2AX foci was also observed (Fig. 1). Therefore, in support of previous reports using non-neuronal cells and other types of cellular stress (23, 24), nuclear localization of STI1 is increased in irradiated astrocytes.

STI1 Levels Regulate Astrocyte Cell Death After Irradiation—To test if STI1 could have a role in the responses of astrocytes to IR, we used astrocytes obtained from STI1 heterozygous knockout mice (21), which present 50% reduction in STI1 levels (Fig. 2*A*). By using Live-Dead staining we

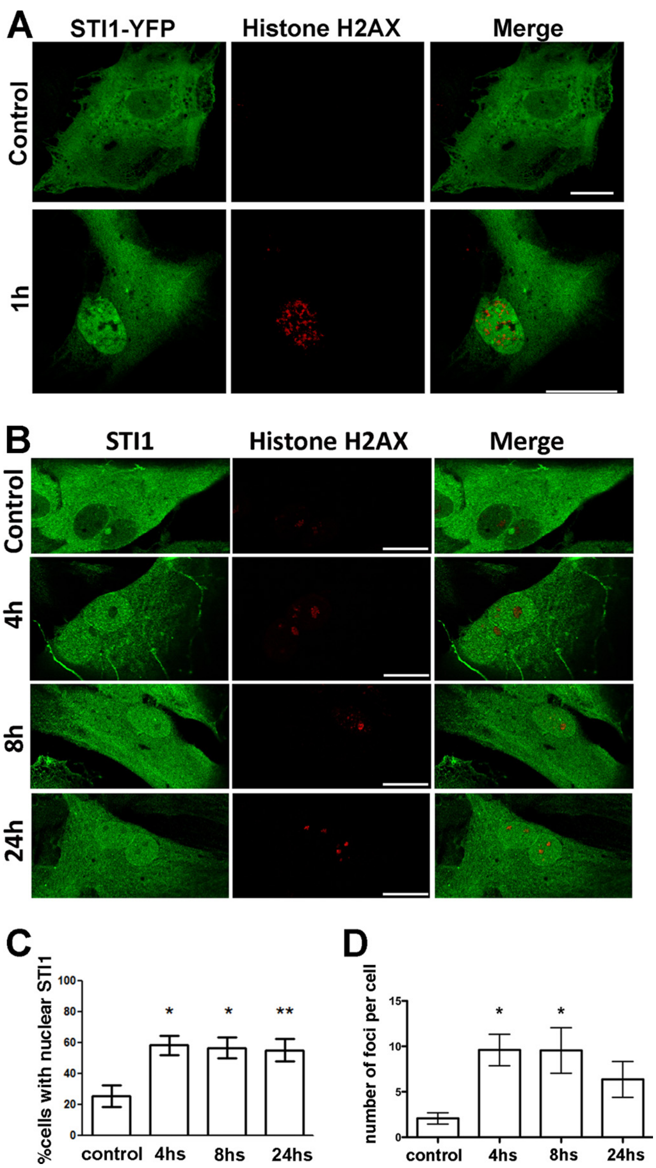

FIG. 1. **Genotoxic stress-induced localization of STI1-YFP or endogenous STI1 to the nucleus.** *A*, Astrocytes were transfected with STI1-YFP. The dishes were placed in a Faxitron RX-650 and subjected to 2Gy of gamma-radiation for 10 min. Cells were fixed at 1 h after irradiation and analyzed by confocal microscopy, the cells presented 30% of transfection efficiency. Foci were detected by anti-H2AX (S139) Alexa Fluor 633. Data are representative of over 50 cells analyzed in four distinct experiments. Scale bars, 20 μm. *B*, Astrocytes were subjected to 2Gy of gamma-radiation for 10 min. Cells were fixed at 4, 8, and 24 h after irradiation and analyzed by confocal microscopy. Endogenous STI1 was detected with anti-STI1 antibody (secondary Alexa Fluor 488) and foci with anti-H2AX (S139), Alexa Fluor 633. *C*, Quantification of percent of cells with nuclear STI1, data was analyzed and compared by one-way ANOVA (p = 0.028), and Newman Keuls post hoc test *, $p < 0.05$. *D*, Quantification of number of foci per cell, data was analyzed and compared by one-way ANOVA (p = 0.0075) and Newman Keuls post hoc test *, $p <$ 0. 05. The images are representative from at least four experiments for each condition, in which at least 50 cells were analyzed. Controls were not irradiated. Scale bars: 12.5 μm.

observed that wild-type astrocytes showed a small, but significant increase in cell death in response to IR (2Gy/10 min, Fig. 2*B* and 2*C*). Interestingly, STI1-deficient astrocytes presented increased cell death in response to irradiation when compared with control astrocytes (Fig. 2*B* and 2*C*). We also measured cell death by determining lactate dehydrogenase (LDH) leakage from dying cells. In this experiment we could not detect a significant increase in LDH leakage from wild-type astrocytes in response to irradiation (Fig. 2*D*), likely because of lower sensitivity of this method. In contrast, astrocytes deficient for STI1 showed increased LDH leakage in response to γ-radiation (Fig. 2 *D*).

Increased nuclear localization of STI1 in response to irradiation suggested a potential role for this protein in genotoxic stress response in astrocytes. To identify potential nuclear targets of STI1, two independent yeast-two hybrid screenings were performed, one using a mouse and the other using a human brain cDNA library. As expected, a number of positive clones encoded for heat shock proteins of the Hsp70 family (Table I), indicating that we were able to identify known interactors of STI1 in the distinct screenings. Interestingly, in both screenings we identified several genes coding for nuclear proteins. These include UBC9, the unique E2 SUMO conjugation enzyme (32); and all members of the PIAS family (PIAS1, PIAS2, PIAS3 and PIAS4), which have SUMO E3 ligase activity and also function as transcription and repression factors (33, 34). Pc2, a polycomb protein that has E3 SUMO ligase activity and is involved with DNA repair (35), was also isolated in the screening (Table I). Although other cDNAs were also identified, we focused further work on genes related to the SUMOylation pathway.

To investigate the functional significance of these potential interactions we examined the colocalization of these proteins with STI1-YFP fusion constructs (36) in CF-10 cells because of their neuronal-precursor like features (13). STI1-YFP is localized mainly in the cytoplasm of CF-10 cells (Fig. 3*A*), as previously described in other cell lines (23). In contrast, UBC9, Pc2 as well as PIAS1 and PIAS4 (Fig. 3A), used as representatives of the PIAS family, show a predominant nuclear localization. Interestingly, cotransfection of PIAS1 with STI1-YFP led to increased nuclear localization of STI1-YFP in cells (Fig. 3*B*) and colocalization between STI1 and PIAS1. In contrast, transfection of PIAS4, Pc2 and UBC9 did not affect the localization of STI1 (Figs. 3*C*, 3*D*, and 3*E* respectively). Quantification of fluorescence intensity showed that the nuclear/cytoplasmic (N/C) STI1 ratio was significantly increased with overexpression of PIAS1, but not PIAS4 (Fig. 3*F*).

Localization of STI1, PIAS1 and UBC9 in astrocytes showed essentially the same pattern observed in CF-10 cells (compare Fig. 3 to Fig. 4). Moreover, overexpression of PIAS1 resulted in increased localization of STI1-GFP in the nucleus and colocalization of PIAS1 with STI1-GFP is astrocytes (Fig. 4*B*). Nuclear retention of endogenous STI1 was also increased by overexpression of PIAS1, but not by overexpres-

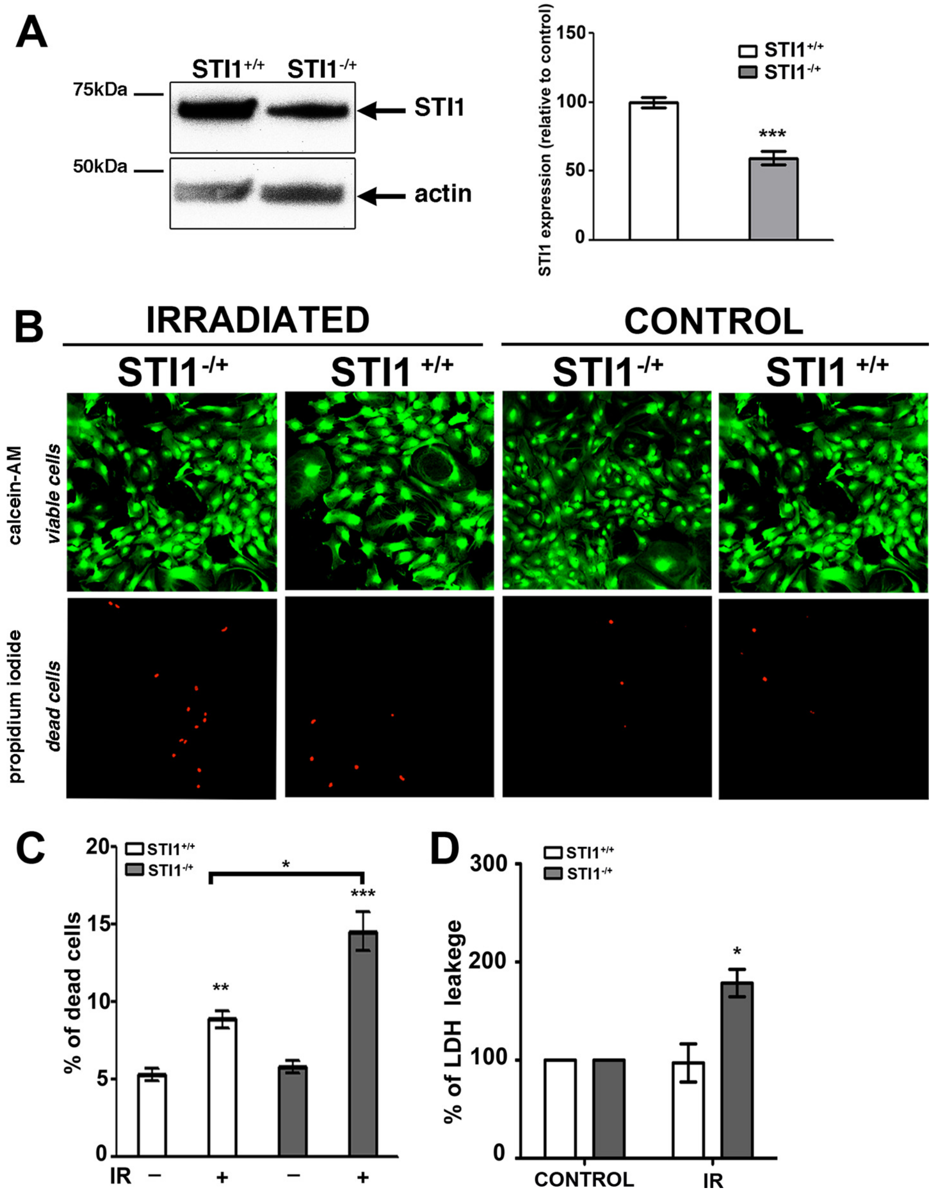

FIG. 2. **STI1 levels influence astrocyte death after irradiation.** *A*, Western blot representing STI1 expression in primary culture of astrocytes obtained from STI1$^{+/+}$ and STI1$^{-/+}$ mice. *B*, Primary culture of astrocytes obtained from STI1$^{+/+}$ and STI1$^{-/+}$ mice were submitted to 2Gy of gamma-radiation for 10 min (20Gy of IR). Cells were stained 48 h later by using live/dead kit (green live cells/red dead cells) or had their cultured media collected for LDH release assay after 48 h. Representative images of astrocytes stained using the live/dead kit in the indicated conditions. *C*, Quantification of cell death in four independent experiments. *D*, LDH release in four independent experiments for the indicated conditions. Data were analyzed and compared by one-way ANOVA (p = 0.0002) with Newman-Keuls post hoc test ***, $p < 0.0001$ **, $p < 0.001$ and *, $p < 0.01$.

sion of UBC9 (Figs. 4*C* and 4*D*, respectively) in primary culture of astrocytes. Colocalization of endogenous STI1 with overexpressed PIAS1 was even more striking and most cells in which PIAS1 was overexpressed showed predominant nuclear localization of STI1, in contrast to its cytosolic localization in astrocytes not overexpressing PIAS1 (Figs. 4*C* and 4*A*). Quantification of the results for images obtained in several dishes from distinct cultures shows a Manders M average coefficient of colocalization for PIAS1 and STI1 with values of M1 = 0.963 ± 0.070 (mean ± S.D.) and M2 = 0.976 ± 0.400 (mean ± S.D.), respectively, indicating strong colocalization between the two fluorescent channels.

PIAS1 has been shown to be present in PML bodies, which are sites of protein-protein interaction in the nucleus (37–40). To determine if STI1 could also be present in PML bodies in PIAS1 overexpressing astrocytes we transfected these cells with PIAS1 and PML-YFP and monitored the localization of endogenous STI1. The results show that part of the endogenous STI1 accumulates in PML bodies only in PIAS1 transfected cells (Figs. 5*A* and 5*B*, arrowheads). Quantification of

TABLE I
Clones from cDNA Libraries

Clones isolated from cDNA Libraries with STI1 bate		
Isolated clones	Number of clones isolated in the human brain library	Number of clones isolated in the mouse brain library
Heat shock protein 70 (***HSP70***)	5	5
Melanoma antigen family D, 4 (***MAGED4***)	2	–
Fasciculation and elongation protein zeta 2 (***FEZ 2***)	3	2
Protein inhibitor of activated STAT 3 (***PIAS3***)	2	–
Protein inhibitor of activated STAT 2 (***PIAS2***)	–	1
Protein inhibitor of activated STAT 1 (***PIAS1***)	–	1
Protein inhibitor of activated STAT 4 (***PIAS4***)	–	2
Ubiquitin conjugating enzyme E21 (***UBC9***)	4	14
Heat shock protein 8 (***HSP8***)	–	36
Chromobox homolog 4 (***PC2***)	–	20
Laminin, beta 2 (***Lamb2***)	–	2
RAS protein-specific guanine nucleotide-releasing (***Rasgrf1***)	–	14
Chromodomain helicase DNA binding protein 3 (***Chd3***)	–	4
E3 ubiquitin protein ligase.HECT (Edd1) (***UBR5***)	–	1
Homeodomain-interacting protein kinase 2b (***HIPK2***)	–	2

images from multiple cells showed colocalization of STI1 and PML bodies in the presence of PIAS1 (0.28 $\pm$ 0.03, Mean $\pm$ S.E.) when compared with cells in which PIAS 1 was not overexpressed (0.09 $\pm$ 0.02, Mean $\pm$ S.E.; $p < 0.001$ when the two colocalization indexes are compared). Moreover, because STI1 can biochemically and functionally interact with Hsp90 we examined the localization of this chaperone in astrocytes. STI1-GFP and Hsp90 show extensive colocalization in astrocytes mostly in the cytoplasm (Fig. 5*C*). Remarkably, increased expression of PIAS1 caused both STI1 and Hsp90 to be in the nucleus (Fig. 5*D*). Furthermore, colocalization analysis in several images from distinct dishes suggest that STI1, Hsp90 and PIAS1 colocalize in the nucleus of PIAS1 overexpressing astrocytes (Manders colocalization coefficient of M1 = 0.92 $\pm$ 0.10 and M2 = 0.93 $\pm$ 0.09 (mean $\pm$ S.D.) for Hsp90 and STI1 and M1 = 0.89 $\pm$ 0.10, M2 = 0.83 $\pm$ 0.20 for Hsp90 and PIAS1. Manders M coefficient of M1 = 0.98 $\pm$ 0.05 and M2 = 0.92 $\pm$ 0.20, for STI1-GFP and PIAS1-Myc respectively.

PIAS1 is a SUMO E3 ligase and it is well known that SUMOylation can increase nuclear localization and retention of proteins (41–43). We envisioned two potential mechanisms by which augmented expression of PIAS1 could increase the nuclear localization/retention of STI1: (1) PIAS1 could SUMOylate STI1, which would lead to its increased nuclear retention; (2) PIAS1 and STI1 could interact directly and this interaction would serve to retain nuclear translocated STI1 into the nucleus. To discriminate between these two possibilities we first determined if STI1 could be SUMOylated. We performed *in vitro* SUMOylation assays using recombinant STI1, UBC9 and SUMO1, SUMO2, and SUMO3. ATP-dependent SUMOylation of STI1 *in vitro* was observed as an upward shift in the apparent molecular mass of the protein, with several SUMOylated species of STI1 being detected (Fig. 6*A*, arrowheads, small protein fragments lower than STI1 are likely proteolytic products). This experiment showed that UBC9 can poly-SUMOylate STI1 *in vitro* in the absence of any E3-ligase and that SUMO1, 2, and 3 can all be used to SUMOylate STI1 (Fig. 6*B*). To further investigate STI1 SUMOylation in cells, and test the possibility that PIAS1 could function as E3-ligase for STI1, we conducted assays in HEK 293 cells overexpressing SUMO and PIAS1. Extracts from cells cotransfected with SUMO1, PIAS1 and STI1-HA were immunoprecipitated using an antibody against HA and immunoprecipitated material (Fig. 6*C*) as well as cell lysates (Fig. 6*D*) were analyzed by Western blotting. Immunoprecipitates from cells transfected with STI1 and SUMO1 showed SUMOylated STI1 species (Fig. 6*C*), which were more pronounced when PIAS1 was cotransfected with SUMO1 and STI1. Similar results were obtained when cells were transfected with STI1 and SUMO3 (not shown). STI1 SUMOylated bands were also detected with SUMO antibodies (arrowheads Fig. 6*C*), suggesting that indeed PIAS1 can act as an E3-ligase for STI1. PIAS1 and presumably SUMOylated PIAS1 were also coimmunoprecipitated with STI1 in this condition (Fig. 6*C*, anti-Myc). The different species of SUMOylated STI1 could be easily and specifically identified in cell extracts using the STI1 antibody (Fig. 6*D*, anti-STI1).

STI1 SUMOylation Sites—Our data indicated that STI1 can be poly-SUMOylated, therefore we used bioinformatic analysis to identify potential STI1 SUMOylation sites. Our analysis indicated the presence of 62 potential SUMOylation consensus site (using SUMOsp 2.0 software). To determine the precise location of modified lysine residues on STI1, we performed an *in vitro* SUMOylation assay using a His-tagged form of SUMO3 that facilitates the identification of SUMOylation sites (44). STI1 was incubated in the presence of UBC9, SAE1/2, Mg/ATP, and this SUMO3 form, and proteins were subsequently digested with trypsin and analyzed by LC-MS/MS to identify modified tryptic peptides bearing the remnant side chain from the mutant SUMO3. Confirmation of modified residues was obtained from the high resolution HCD MS/MS

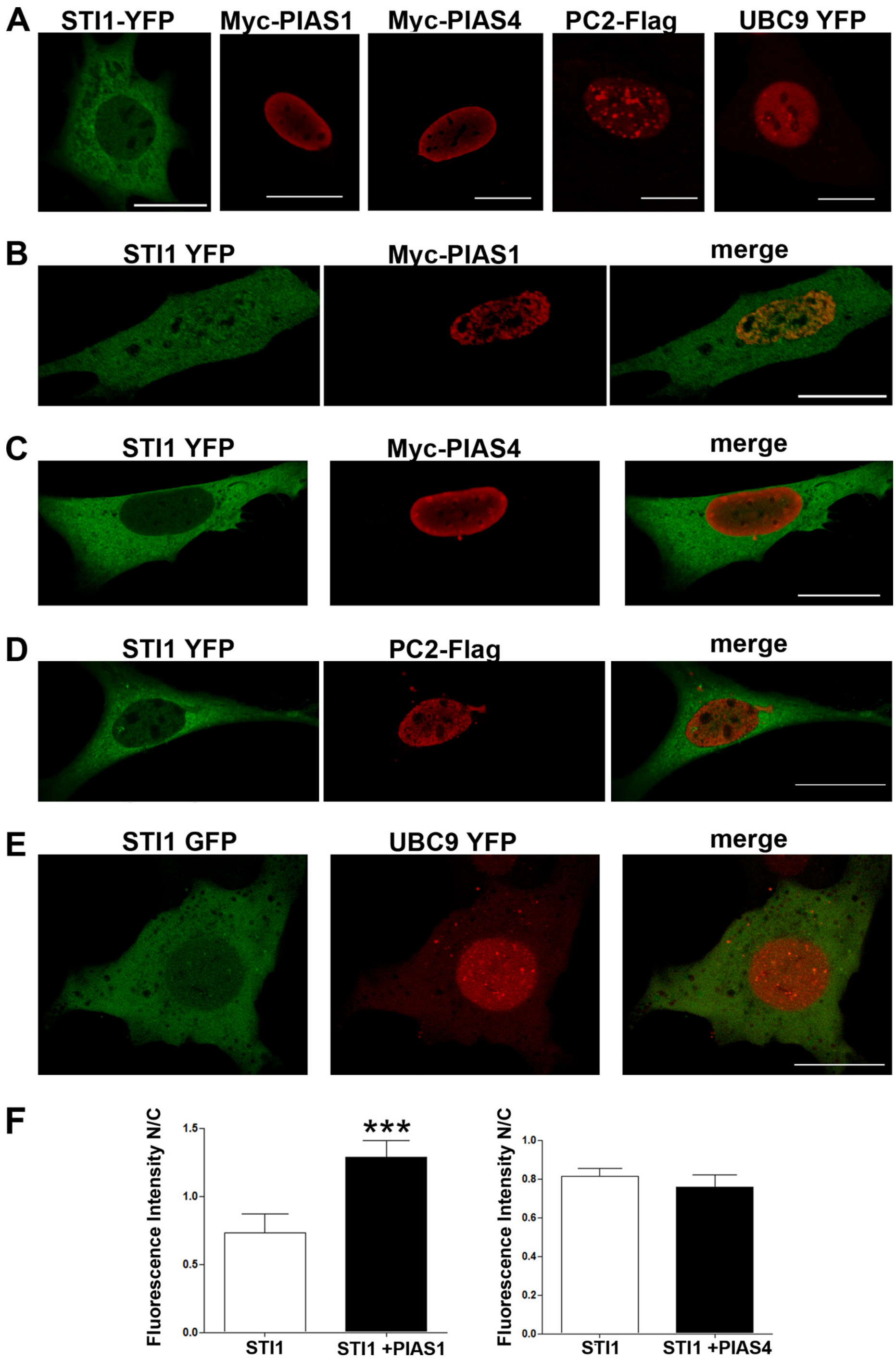

FIG. 3. **PIAS1 expression in CF10 cells increases the retention of STI1-YFP in the nucleus.** CF10 cells were transfected with indicated constructs and 48 h later cells were imaged by confocal microscopy. *A*, Representative images of cells individually transfected with the indicated constructs. *B–E*, Representative image of cells co-transfected with: STI1-YFP and PIAS1-Myc (*B*), STI1-YFP and PIAS4-Myc (*C*), STI1-YFP and PC2-FLAG (*D*) and STI1-GFP and UBC9-YFP (*E*). *F,* Quantification of STI1 nucleus/cytoplasm ratio in cells overexpressing PIAS1 or PIAS4, note significant increase of nuclear STI1 with PIAS1 overexpression. These cells presented an average of 50% of transfection efficiency. Images are representative from at least four experiments for each condition, in which at least 50 cells were analyzed. Scale bars, 20 μm. *, p = 0.0381.

spectra of the corresponding tryptic peptides where specific SUMO3 reporter ions were observed at m/z 132.08, 243.11 344.16 (supplemental Fig. S1*A*–S1*E*). These analyses indicated that STI1 is SUMOylated *in vitro* at lysine residues 123, 210, 312, 395, and 486. All these sites are found in regions predicted to be solvent exposed. We then generated a series

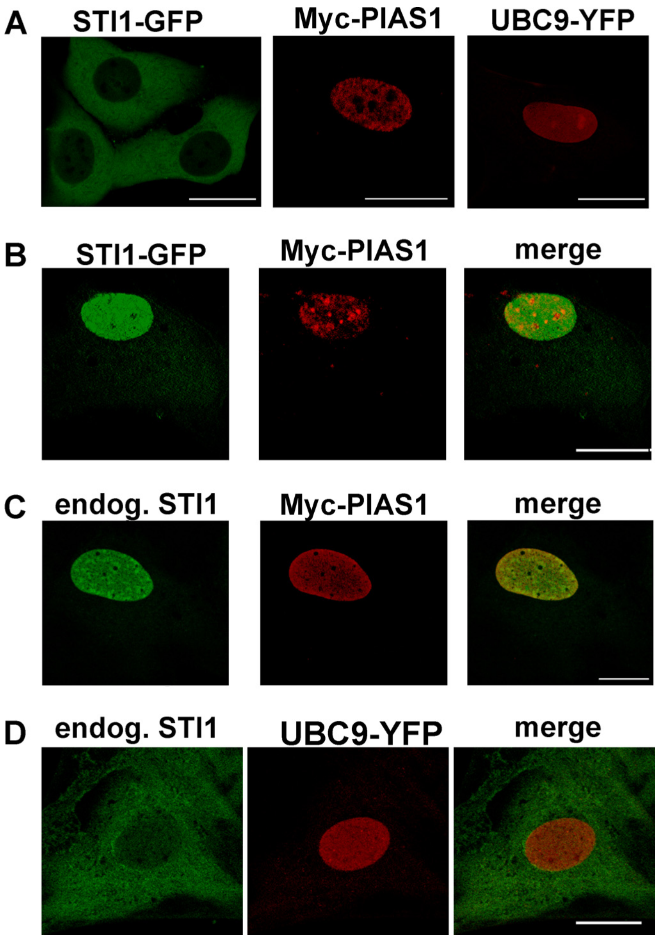

FIG. 4. **PIAS1 expression in astrocytes increases the retention of endogenous STI1 in the nucleus.** Primary cultures of astrocytes were transfected with indicated constructs and 48 h later cells were imaged by confocal microscopy. *A*, Representative images of localization of STI1 and indicated proteins in astrocytes. *B–D*, Representative images of cellular localization of STI1-GFP or endogenous STI1 and indicated proteins in individually transfected astrocytes, there was an average of 40% transfection efficiency. Images are representative from at least four experiments for each condition in which at least 50 cells were imaged. Scale bars, 20 μm. Colocalization analysis was performed, using the ImageJ software, for endogenous STI1 and PIAS1-Myc in the nucleus of cells. The Manders M average coefficient obtained was M1 = 0.963 $\pm$ 0.070 (mean $\pm$ S.D.) and M2 = 0.976 $\pm$ 0.400 (mean $\pm$ S.D.) indicating strong colocalization of STI1 with PIAS1. For this analysis 20 cells were randomly chosen in five independent experiments.

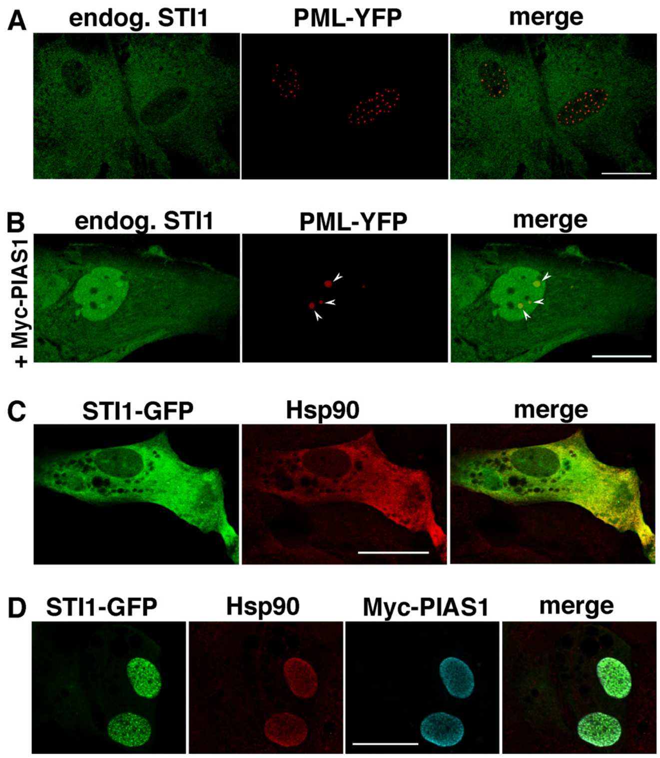

FIG. 5. **STI1 colocalizes with PML-YFP and Hsp90 when PIAS1 is overexpressed.** *A*, Representative image of astrocytes transfected with PML-YFP and stained for STI1. *B*, Representative image of cells transfected with PIAS1 and PML demonstrating colocalization of STI1 with PML NB. *C*, Representative image of astrocytes transfected with STI1-GFP and stained for Hsp90 showing the colocalization and cytoplasmic distribution of the proteins. *D*, Representative image of astrocyte transfected with STI1-GFP and PIAS1-Myc and stained for Hsp90 and Myc. Note that Hsp90 colocalizes well with STI1 in the nucleus of cells expressing PIAS1. The cells presented an average of 30% transfection efficiency. The colocalization between Hsp90 and STI1 or PIAS1 in the nucleus determined with Image J was processed with average Manders colocalization coefficient (mean $\pm$ S.D.): M1 = 0.92 $\pm$ 0.10, M2 = 0.93 $\pm$ 0.09 and M1 = 0.89 $\pm$ 0.10, M2 = 0.83 $\pm$ 0.20 respectively. STI1-GFP and PIAS1-Myc were analyzed as well, and an average Manders M coefficient M1 = 0.98 $\pm$ 0.05, M2 = 0.92 $\pm$ 0.20. A total of 20 cells were randomly chosen from three independent experiments for this analysis. Images are representative of three experiments of each condition in which at least 50 cells were imaged. Scale bars, 12.5 μm.

of lysine (K) to arginine (R) STI1 mutants, including point mutations of each of the SUMOylation sites above, as well as combinations of these mutations. We compared SUMOylation of mutants with SUMOylation of STI1-HA in HEK 293 cell lysates. For these experiments, HEK 293 cell were transfected with SUMO1 and PIAS1, as STI1 is similarly SUMOylated by both SUMO1 and SUMO3 (Fig. 6*A*). To detect only transfected mutated STI1 (mutant or wild-type), we used an anti-HA antibody for the immunoblots. The anti-HA antibody was less effective than the STI1 antibody to detect minor SUMOylated species of STI1, and only the three stronger SUMOylated STI1 bands were detected (supplemental Figs. S1*F* and S1*G*). We detected three main protein bands; whereas the first and second bands ran close together around 120 kDa, the third band showed higher molecular mass (200 kDa). The K123R mutant showed a selective decrease in the first and third bands, whereas the second band seemed preserved (supplemental Fig. S1*F*). In contrast, the intensity of the three SUMOylated STI1 bands was weaker in all the mutants in which K210 was changed (supplemental Figs. S1*F* and S1*G*), suggesting that K210 may provide hierarchal control of STI1 SUMOylation. Individual mutants K312R, K395R,

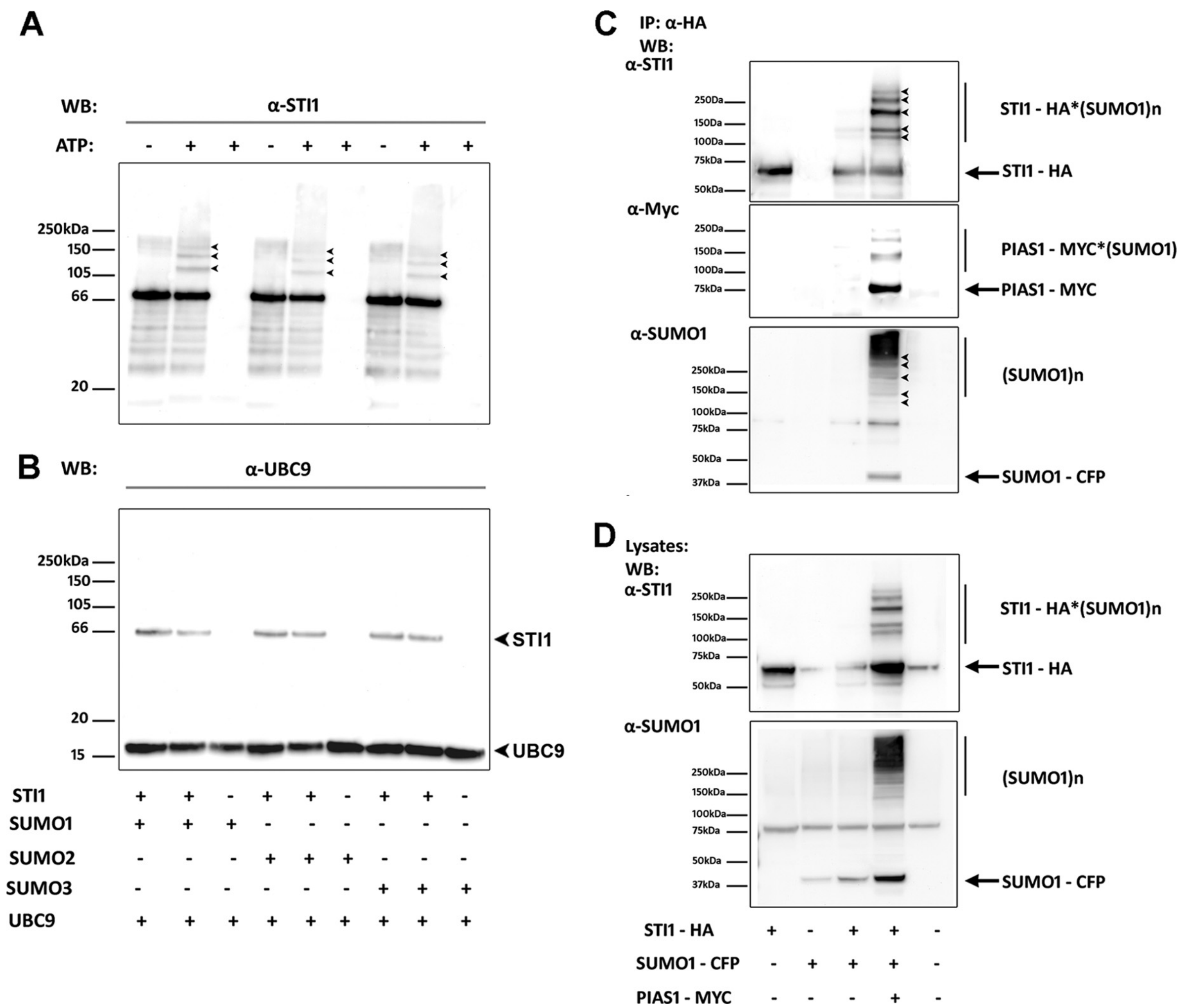

FIG. 6. **STI1 is SUMOylated and PIAS1 is a SUMO E3 ligase for STI1.** Recombinant STI1 was subject to an *in vitro* SUMOylation assay by using recombinant SUMO1, SUMO2, SUMO3, and the SUMO conjugating enzymes SAE1/2 and UBC9. *A*, The higher molecular weight bands detected for STI1 (arrowheads) in the presence of ATP and SUMO1, 2, and 3, indicate that all SUMO isoforms are able to SUMOylate STI1 in an ATP dependent process. *B*, UBC9 expression (arrowhead). *C*, HEK293 cells were cotransfected with HA-STI1, SUMO1 (or SUMO3 - not shown) and PIAS1. STI1 was pulled down using HA agarose beads and blots were processed. IP of STI1 in cells expressing PIAS1 and SUMO1. Arrowheads indicate SUMOylated STI1. *D*, Lysates of cells used in *C*. The data are representative of four experiments.

and K486R did not show large effects on SUMOylated STI1 species (supplemental Fig. S1*G*). A mutant containing changes in these five amino acids (K123–210-312–395-486R) presented impaired SUMOylation (supplemental Fig. S1*F*, arrow, note that the HA antibody does recognize a nonspecific band that migrates close to the SUMOylated STI1 bands).

Following the identification of STI1 SUMOylation sites we assessed whether SUMOylation was responsible for the increased nuclear retention of STI1 on PIAS1 overexpression. For this experiment, we used the STI1 construct with all SUMOylation sites mutated (K123–210-312–395-486R). HA-tagged wild-type STI1 and the mutant STI1 presented similar cytoplasmic localization in astrocytes (Fig. 7*A*). PIAS1 overexpression increased the nuclear retention of both wild-type and mutant STI1 (Figs. 7*B* and 7*C*). Hence, preventing STI1 SUMOylation did not affect its nuclear accumulation, suggesting the possibility that a direct interaction between STI1 and PIAS1, rather than SUMOylation, is responsible for the increased STI1 nuclear localization.

STI1 and PIAS 1 Interact Directly—Yeast-two hybrid screening (Table I) suggested that STI1 and PIAS1 interact directly. Additionally, cotransformation of yeast with a construct containing the N-terminal region of STI1 and PIAS1 cDNA allowed cell growth in restrictive media, whereas no growth was observed in yeast transformed with the empty vector pGBKT7 and PIAS1-pACT2 (not shown), further supporting a direct interaction between these two proteins. To map the interaction sites we generated STI1 and PIAS1 deletion constructs. Multiple regions of STI1 containing the TPR domains were sufficient for interaction with PIAS1 (Fig. 8*A*). In contrast, a specific region in PIAS1 (a.a. 450–480) containing the SUMO-interacting motif (SIM), was required for the inter-

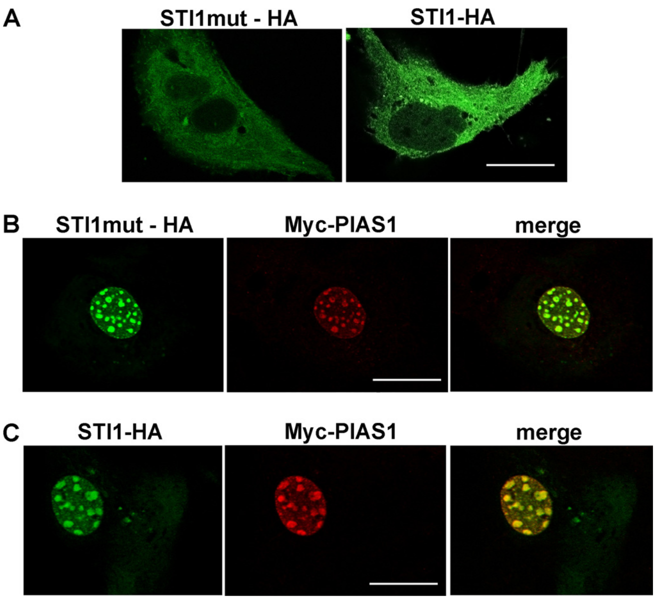

FIG. 7. **STI1 nuclear retention is independent on SUMOylation.** *A*, Representative images for localization of STI1 or a mutant STI1 (K123, 210, 312, 395, 486R) individually transfected in astrocytes. *B* and *C*, Representative images of astrocytes cotransfected with STI1-HA or STI1-HA mutant and PIAS1-Myc. Note that in cotransfected cells the labeling is predominantly nuclear, transfection efficiency was of 30%. Images are representative of at least four independent experiments in each condition in which at least 50 cells were imaged. Scale bars, 12.5 μm.

action with STI1 in the yeast-two hybrid assay (Fig. 8*B*). Substitution of alanine for each of the hydrophobic residues (V457, V459, I460, L462) in the SIM domain of full-length PIAS1 abolished interaction with STI1, whereas mutation of other residues flanking the SIM within aa 450–480 in PIAS1 did not affect the interaction (Fig. 8*C*). These results indicate that in the yeast two-hybrid assay, the SIM in PIAS1 is critical for interaction with STI1. To further confirm the direct interaction of STI1 with PIAS1 we obtained recombinant proteins in bacteria and used surface plasmon resonance (SPR). Full length PIAS1 interacted with full length STI1 immobilized on the SPR chip in a concentration-dependent way (Fig. 8*D*, $K_D = 2.1 \pm 0.2$ μM). A C-terminal peptide (amino acids 450 - 651) containing the SIM domain of PIAS1 interacted with full length STI1 with similar affinity (Fig. 8*E*, $K_D = 2.3 \pm 0.3$ μM). In contrast, a peptide containing only the RING motif of PIAS1 did not interact with full length STI1 (Fig. 8*F*). These results suggest that the two proteins can interact directly and that the C-terminal region of PIAS1 containing the SIM motif is sufficient for this interaction. Our observation that PIAS1 coimmunoprecipitates with STI1 in HEK293 cells (Fig. 6*C*) gives further support for this interaction. To test if STI1 could form a complex with PIAS1 in mammalian cells in the absence of transfected SUMO, we transfected HEK 293 cells only with STI1-HA and PIAS1-Myc. Pull-down of STI1 with HA-beads co-immunoprecipitated PIAS1 (Fig. 8*G*). PIAS1 was not co-immunoprecipitated from HEK 293 cells with anti-HA antibodies when cells were not transfected with STI1-HA, demonstrating specificity.

PIAS1 is Required for Nuclear Retention of STI1 After Genotoxic Stress in Astrocytes—To further determine if the nuclear accumulation of STI1 was indeed because of the interaction with PIAS1, we generated a PIAS1 mutant lacking amino acids 450–480 (PIAS1-MycΔ450–480). Localization of the PIAS1 mutant was indistinguishable from that of wild-type PIAS1 (Fig. 9*A*). Importantly, whereas overexpression of PIAS1 induces nuclear accumulation of STI1, overexpression of the mutant does not (Figs. 9*B* and 9*C*).

To test whether PIAS1 plays a role in the nuclear retention of STI1 in response to IR, we used siRNA to knockdown PIAS1 in astrocytes (Fig. 10). siRNA transfection decreased PIAS1 expression by 75% and abolished immunostaining of PIAS1 in the nucleus of astrocytes (Figs. 10*B* and 10*C*, respectively), whereas a control scrambled siRNA had no effect on PIAS1 expression when compared with nontransfected astrocytes (Figs. 10*A*–10*C*). Irradiated astrocytes transfected with PIAS1 siRNA presented STI1 mainly in the cytoplasm (Fig. 10*D*). A correlation analysis indicated a relationship between PIAS1 levels and STI1 nuclear localization (Fig. 10*E*). These results indicate that retention of nuclear STI1 after irradiation depends on its interaction with PIAS1 in the nucleus.

GBMs Express Higher Levels of PIAS1 and Nuclear STI1 than Non-neoplasm Samples—To evaluate the potential significance of increased PIAS1 expression and STI1 nuclear localization in astrocytes, we evaluated these proteins in GBM, the most aggressive and common CNS tumor in adults. GBMs present altered DDR (45) and are fairly resistant to irradiation (46). IHC analysis showed that PIAS1 is expressed only in the nucleus of GBM samples (Fig. 11*A*), whereas STI1 is highly expressed in the cytoplasm of non-neoplasm and tumor cells (Fig. 11*C*). Remarkably, GBMs presented higher PIAS1 expression (Fig. 11*B*) and an increment of STI1 nuclear localization (Fig. 11*D*), when compared with normal brain tissue. Furthermore, there was a significant positive correlation among GBMs with higher levels of PIAS1 expression and increased STI1 nuclear localization ($r = 0.364$, $p < 0.0005$). These findings are consistent with our observations in astrocytes suggesting that PIAS1 can modulate nuclear STI1 localization.

DISCUSSION

We show that decreased levels of STI1 increase the sensitivity of astrocytes to γ-radiation-induced cell death, suggesting a role for STI1 in response to this specialized form of stress. Our data show that STI1 is retained in the nucleus in response to γ-irradiation and we identified several nuclear proteins that can interact with STI1. Functional overexpression assays identified PIAS1, a critical nuclear protein that regulates the DDR and gene transcription (47, 48), as a direct interactor for STI1. Although PIAS1 has E3-ligase activity

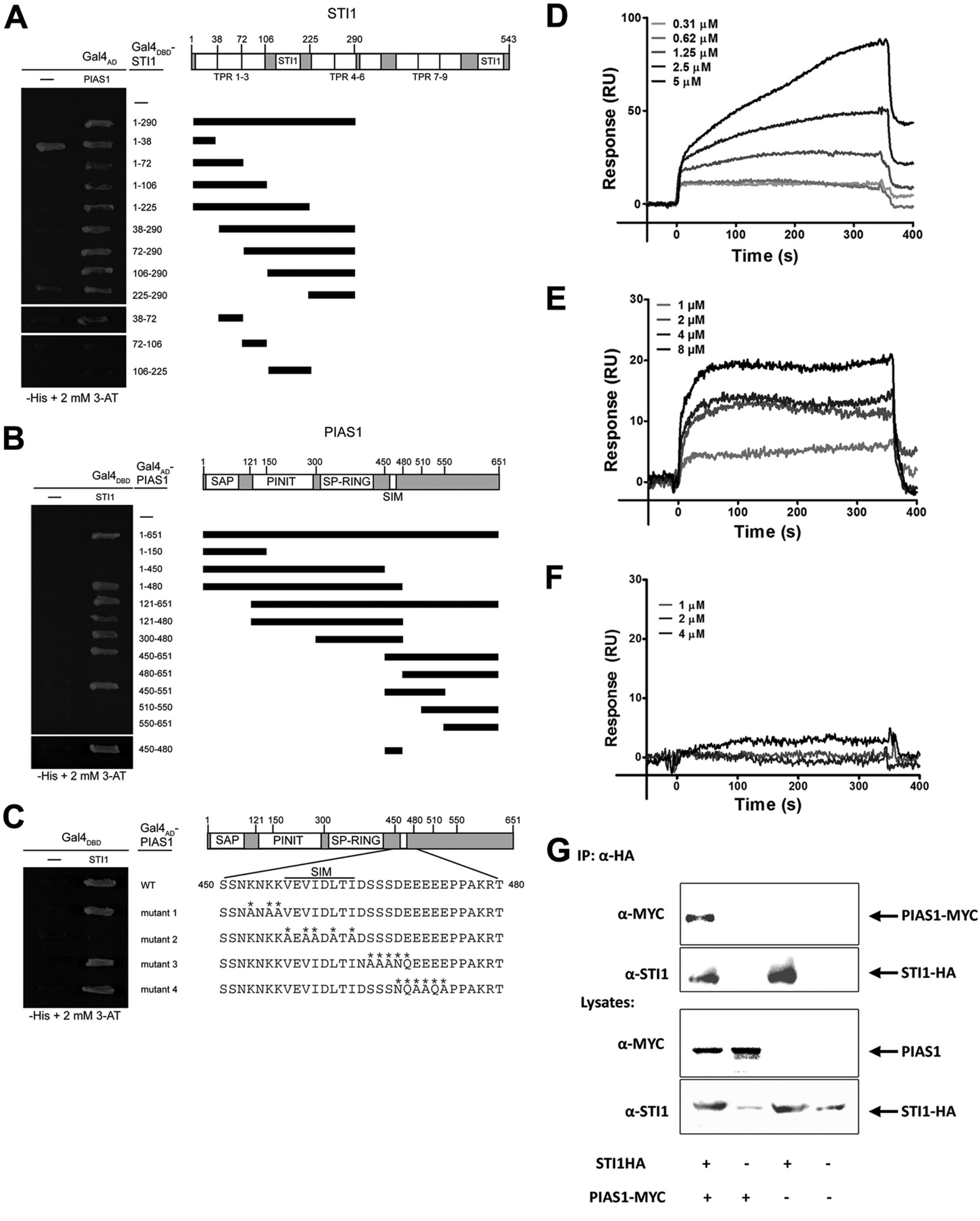
A
STI1
1 38 72 106 225 290 543
STI1
STI1
TPR 1-3
TPR 4-6
TPR 7-9
Gal4AD
Gal4DBD-STI1
—
PIAS1
1-290
1-38
1-72
1-106
1-225
38-290
72-290
106-290
225-290
38-72
72-106
106-225
-His + 2 mM 3-AT
B
PIAS1
1 121 150 300 450 480 510 550 651
SAP
PINIT
SP-RING
SIM
Gal4DBD
Gal4AD-PIAS1
STI1
1-651
1-150
1-450
1-480
121-651
121-480
300-480
450-651
480-651
450-551
510-550
550-651
450-480
-His + 2 mM 3-AT
C
Gal4DBD
Gal4AD-PIAS1
STI1
WT
mutant 1
mutant 2
mutant 3
mutant 4
SIM
450 SSNKNKKVEVIDLTIDSSSDEEEEEPPAKRT 480
SSNANAAVEVIDLTIDSSSDEEEEEPPAKRT
SSNKNKKAEAADATADSSSDEEEEEPPAKRT
SSNKNKKVEVIDLTINAAANQEEEEPPAKRT
SSNKNKKVEVIDLTIDSSSNQAAQAPPAKRT
-His + 2 mM 3-AT
D
0.31 μM
0.62 μM
1.25 μM
2.5 μM
5 μM
Response (RU)
Time (s)
E
1 μM
2 μM
4 μM
8 μM
Response (RU)
Time (s)
F
1 μM
2 μM
4 μM
Response (RU)
Time (s)
G IP: α-HA
α-MYC
α-STI1
PIAS1-MYC
STI1-HA
Lysates:
α-MYC
α-STI1
PIAS1
STI1-HA
STI1HA + - + -
PIAS1-MYC + + - -

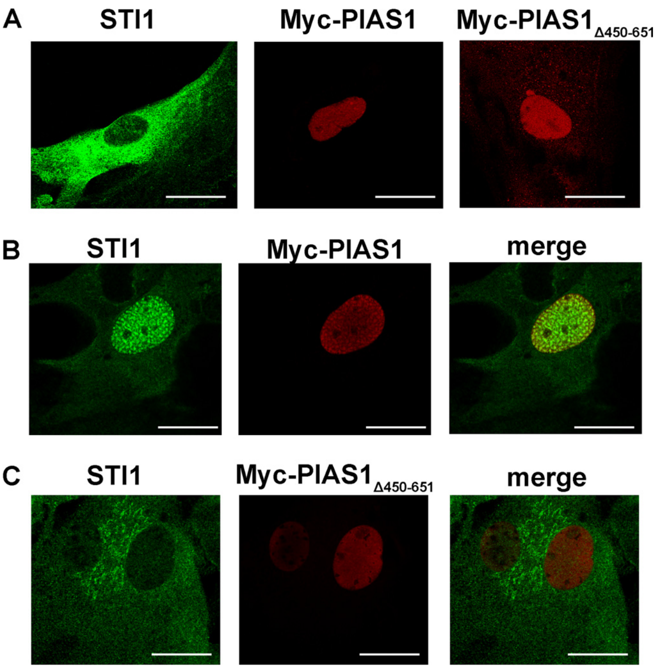

FIG. 9. **Overexpression of mutant PIAS1 does not retain STI1 in the nucleus.** *A*, Astrocytes were transfected with either PIAS1 or PIAS1$_{\Delta450-480}$-Myc and imaged. *B*, Astrocytes were transfected with PIAS1-Myc and endogenous STI1 (green) or Myc (red) were imaged. *C*, Astrocytes were transfected with PIAS1$_{\Delta450-480}$-Myc and STI1 (green) or Myc (red) were imaged. The cells presented a transfection efficiency of 30%.

toward STI1, we demonstrated that STI1 nuclear accumulation is independent of its SUMOylation, but it seems to depend on the interaction between STI1 and PIAS1. This interaction requires multiple domains on STI1 and the SIM domain on PIAS1. Our biochemical experiments however show that the two proteins can interact independently of SUMOylation. Importantly, localization of STI1 in the nucleus in response to γ-irradiation depends on PIAS1, suggesting that PIAS1 is a novel interacting partner for STI1 that promotes its nuclear retention during genotoxic stress.

It seems that a number of proteins involved in signaling for canonical DDR response, such as ATM and p53, play less important roles in astrocytes when compared with cancer cells (26). Furthermore, it has been shown that astrocytes do not activate apoptosis in response to irradiation (26). Although we did not examine apoptosis, our results are compatible with these previous observations, and show that wild-type astrocytes are indeed highly resistant to IR. Using the Live-Dead assay we were able to detect a small, but significant increase in astrocyte cell death after IR. Importantly, astrocytes isolated from STI1 heterozygous knockout mice showed increased cell death after γ-irradiation when compared with wild-type astrocytes, suggesting the possibility that STI1 is involved in modulating cell survival in response to DNA damage. These results are in agreement with previous observations showing that knockdown of STI1 specifically sensitizes YAC-1 cells (mouse lymphoma cells) to irradiation mediated cell death (25).

Nuclear accumulation of STI1 in response to IR in astrocytes was fast (within minutes), persisted for at least 24 h and was dependent on PIAS1 expression. Interestingly, although it is known that STI1 accumulates in the nucleus of cell lines in response to other types of cellular stress (23), its nuclear functions are poorly understood. STI1 has both nuclear localization signals (*e.g.* a.a. 222–239) and nuclear export signals (23). Inhibition of nuclear export of proteins with leptomycin B increases the localization of STI1 in the nucleus, suggesting that the protein normally shuttles between nuclear and cytoplasmic locations (23).

Nuclear STI1 did not appear to be initially recruited to DNA breaks, as it did not colocalize with γ-H2AX foci (Fig. 1), a marker of DNA damage. Thus, the pattern of STI1 nuclear localization is not completely identical to that of PIAS1, which is recruited to sites of DNA damage (48). However, PIAS1 has also been found to colocalize with PML in PML nuclear bodies (NB) (49); thus the STI1-PIAS1 interaction may serve to direct STI1 to specific locations in the nucleus (such as PML NBs) or to specific client proteins. In agreement with the potential for STI1 to act as a cochaperone when recruited by PIAS1, Hsp90 was also recruited to the same sites.

STI1 was previously reported to function in DNA damage/repair pathways as a cochaperone for CHK1 (50) and the DNA repair protein Ssl2, the yeast homolog of XPB (51), a DNA helicase that can function in DNA repair pathways. Interestingly, a recent report pointed out that CHK1 activation in

Fig. 8. **STI1 interacts with PIAS1.** *A–C*, Yeast cotransformed with plasmids directing expression of the indicated fusion proteins, or vector with no insert (-), were patched onto solid medium lacking histidine and supplemented with the histidine analog 3-amino-1,2,4-triazole (3-AT), and interaction of the fusion proteins was assessed based on growth of yeast after incubation at 28 °C for 5 days. Positions of truncation points or point mutations relative to functional domains in PIAS1 and STI1 are indicated. *D*, Kinetics of PIAS1 peptides binding to STI1 immobilized on a CM5 chip were followed by surface plasmon resonance (SPR) signal using Biacore X system (GE, USA). Graph showing binding curves for the full-length PIAS1 (a.a. 1–651). Darkening shades of gray represent increasing (0.31 to 5 μM) concentrations of full-length PIAS1. "On" and "off" kinetics were analyzed as described in Methods to give $K_D = 2.1 \pm 0.2$ μM, $k_{off} = 0.23 \pm 0.02$ s^{-1} and $k_{on} = 1.1 \pm 0.1 \times 10^5$ M^{-1}·s^{-1}. *E*, The same for the C-terminal PIAS1 peptide (a.a. 451–651). Darkening shades of gray represent increasing (1 to 8 μM) concentrations of C-terminal PIAS1. $K_D = 2.3 \pm 0.3$ μM, $k_{off} = 0.19 \pm 0.04$ s^{-1} and $k_{on} = 8.3 \pm 2.0 \times 10^4$ M^{-1}·s^{-1}. *F*, Injections of 1 to 4 μM PIAS1 RING domain (a.a. 300–450) did not cause significant SPR signals. Binding curves are representatives from three independent experiments. *G*, Representative immunoblots showing co-immunoprecipitation of PIAS1 with STI1 from HEK293 cells. HA-STI1 was precipitated with anti-HA beads and specific antibodies were used to detect STI1 or Myc (PIAS1). The data are representative of four independent experiments for each condition.

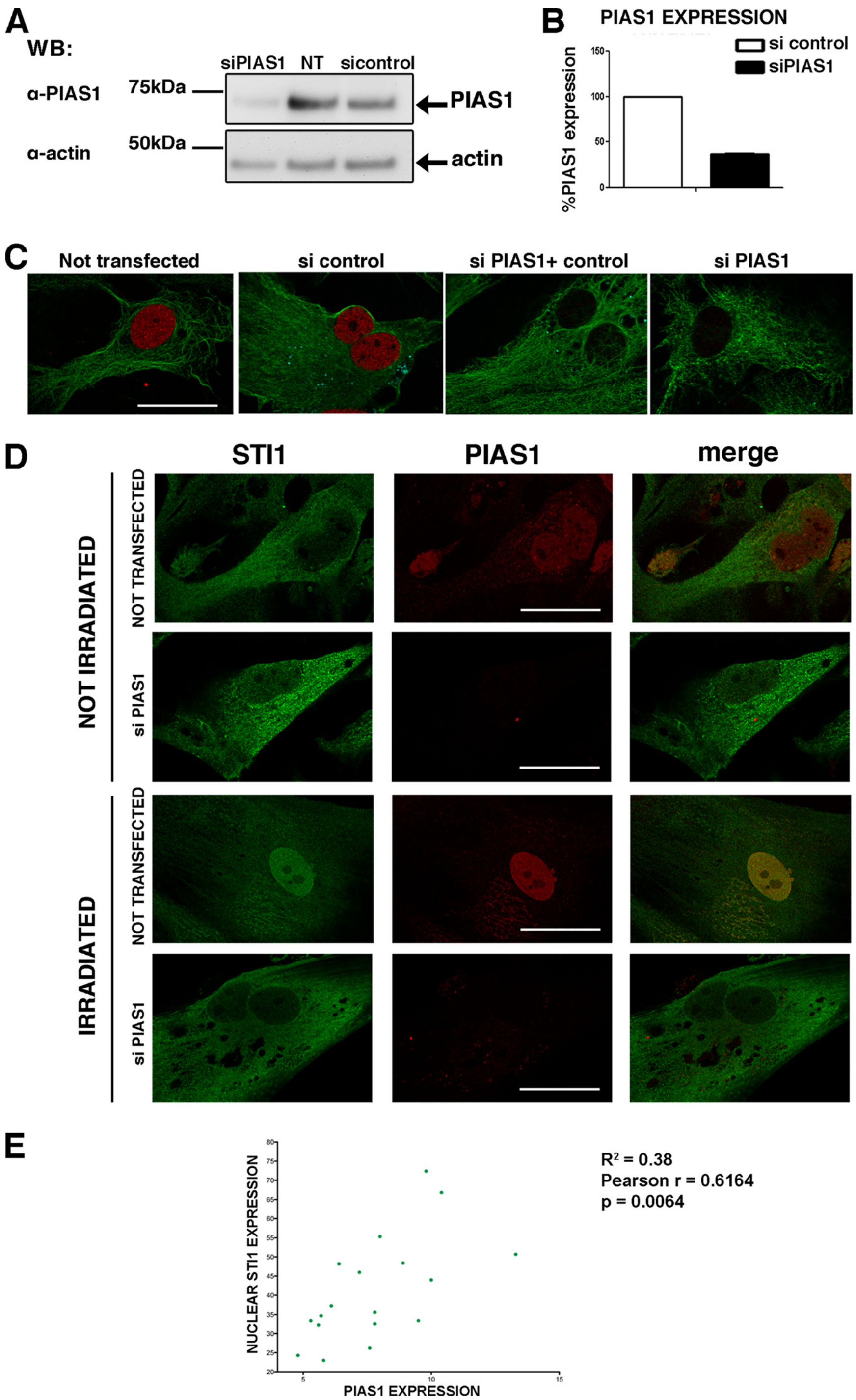

FIG. 10. **STI1 retention in the nucleus after genotoxic stress is dependent on PIAS1 expression.** *A*, Expression of PIAS1 in control astrocytes, astrocytes transfected with PIAS1 or control siRNA. *B*, Western-Blot quantification of PIAS1 expression in siRNA-transfected astrocytes. *C*, PIAS1 expression determined by immunolocalization in astrocytes transfected with the indicated siRNA. Green staining represents anti-β tubulin used to determine cell morphology. Note that transfection of control siRNA has no effect on PIAS1 expression. *D*, Cellular distribution of STI1 and expression of PIAS1 in control or irradiated astrocytes, the cells presented a tranfection efficiency of 30%. *E*, Irradiated cell transfected with siRNA for PIAS1 were quantified for nuclear STI1 and PIAS1 expression and a correlation between the levels of PIAS1 expression and nuclear STI1 was determined. Nuclear localization of STI1 was correlated to decreased PIAS1 expression. $R^2 = 0.38$, Pearson $r = 0.6164$ and $p = 0.0064$. Data are representative of three independent experiments for each condition in which >50 cells were imaged and analyzed. Scale bars, 25 μm.

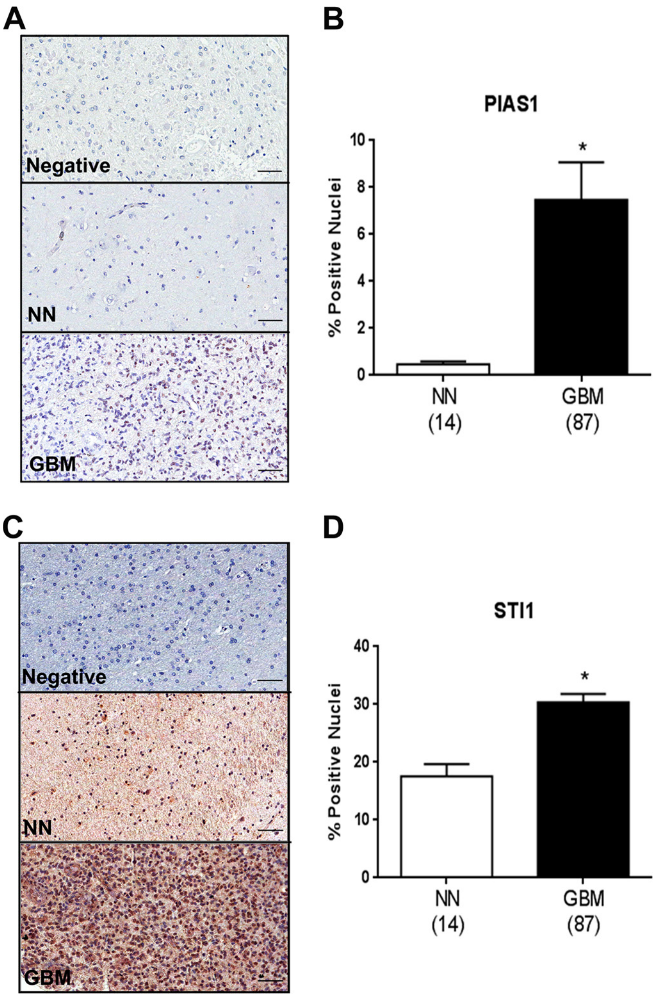

FIG. 11. **Expression of PIAS1 and STI1 in GBMs.** (*A*, *C*) Representative IHC staining in GBM and non-neoplasm samples (NN) for PIAS1 and STI1 respectively. *B*, Quantification of PIAS nuclear localization in GBMs compared with NN. *D*, Quantification of STI1 nuclear localization in GBMs compared with NN. Scale bars, 50 μm. Negative means a tumor slide stained only with secondary antibody, developed and counterstained as described for STI1 and PIAS1. Numbers between brackets represent the total number of samples. *, $p < 0.05$ Student's *t* test.

response to DNA damage is dependent on the integrity of PML NBs (52). Although the failure to activate CHK1 in response to DNA damage may be as a result of impaired ssDNA formation in PML depleted cells (52), it is tempting to speculate that PML NBs localization could facilitate STI1 interaction with CHK1.

PML NBs are populated by various factors involved in DNA repair, cell cycle checkpoint and apoptosis and have emerged as important regulators of the DDR (38, 53). Several reports have described the relocalization of a number of proteins to PML NBs in response to DNA damage, including p53 (54), IKK family member IKKε (55) and Mre11 (56). We have recently shown that loss of STI1 causes a decrease in the levels of p53 (21). Although functioning in distinct pathways, these proteins all have in common a protective function against the threat of DNA damage. PML bodies serve also as sites for accumulation of SUMOylated proteins. We show that STI1 is SUMOylated and defined five SUMOylation sites on STI1. The precise role of STI1 SUMOylation on STI1 cochaperone activity will need to be studied in the future. However, STI1 SUMOylation is not required for its nuclear retention. It is likely that on recruitment of STI1 to the nucleus, the interaction of STI1 with PIAS1 will allow for SUMOylation of the former, which may help STI1 to regulate its nuclear interaction network.

Consistent with the possibility that STI1 may serve as a cochaperone in the nucleus, we found that Hsp90 colocalized with nuclear STI1. Interestingly, elimination of embryonic STI1 is lethal likely because of loss of Hsp90 client proteins such as Grk2, STAT3 and p53 (21), without changes in the levels of Hsp90. Nuclear Hsp90 has recently emerged as a regulator for the DDR (57). Phosphorylation of Hsp90 by IR led to its accumulation in γ-H2AX foci and knockdown of Hsp90 led to less efficient DNA repair as well as a decrease in γ-H2AX foci with both events occurring concomitantly 3 h after irradiation (57). Moreover, BRCA1, a critical protein involved in DSBs has recently been shown to be a Hsp90 client (58).

There are different subtypes of human brain tumors, however GBMs are the most aggressive and common tumors in the adult CNS. These tumors are highly proliferative, present diffuse infiltration, propensity for necrosis and robust neovascularization. Despite their histological similarities GBMs have recently been suggested to represent heterogeneous diseases (59). Therapeutic options to approach these tumors increased in the last years, nevertheless the prognosis is still poor (60). We show here that GBMs express higher levels of PIAS1. In agreement with results in mouse astrocytes, we detected a positive correlation between increased levels of PIAS1 and increased nuclear STI1 in GBMs, suggesting the possibility of pathological relevance for the interaction we described. It is known that mTOR signaling is one of the key pathways altered in GBMs and resistance to mTOR inhibitors has been associated to PML overexpression (61). Nuclear PMLs can be regulated by arsenic trioxide, a drug used to treat acute promyelocytic leukemia (62) and also proposed to be used in GBMs (61). This agent is known to induce PML-NB SUMOylation followed by polyubiquitination and proteasomal degradation (62) or to modulate sequestration of PMLs in cytoplasmic complexes of PML and nucleoporins (63). Our data showed that STI1 colocalizes with PML-NB when PIAS1 is overexpressed. It is unknown if the complex STI1/PIAS1 can modulate PML-NB SUMOylation or have any chaperone activity on PML-NB, but this possibility deserves further investigation.

The precise role for nuclear STI1 in irradiation and particularly its consequences in GBM treatment with radiotherapy will need to be further explored, but few possibilities can be envisioned. Some of the subnuclear structures, such as PML NB, that have crucial functions in the DDR present high levels of accumulated proteins (40). Having functional Hsp90-STI1 chaperone machinery in the nucleus may allow higher concentration of client proteins in these structures without promiscuous interactions or formation of higher order aggregates. Indeed, STI1 has been shown in yeast to cure prions via Hsp104 (64), a mechanism that is not well understood, but may depend at least in part on protein disaggregation. Moreover, in the absence of embryonic STI1 cells present increased γ-H2AX sites and commit to apoptosis (21). In agreement with the notion that STI1 may indirect affect DNA repair, p53, a Hsp90 client, is decreased by 50% in embryos lacking STI1 (21). Interestingly, interference with the interaction between STI1 and Hsp90 induces cytotoxicity in GBM cell lines, by reducing levels of p53 and other Hsp90 client proteins (65). STI1 may also serve as a scaffold for bridging Hsp90 to other proteins, as recently suggested for regulation of Piwi and its piRNAs in canalization mechanisms in *Drosophila* (66). Our results provide a novel mechanism for interplay among STI1, Hsp90, PIAS1, and DNA damage in astrocytes. Further identification of interactions of STI1 and nuclear proteins may shed new light on multiple functions of STI1 as a cochaperone protein and scaffolding molecule.

Acknowledgments—We thank Drs. David Wotton, Lienhard Schmitz, and Marc Tini for reagents as well as Dr. Dale Laird for reading and suggestions in an earlier version of this manuscript. VRM, VFP, and MAMP would like to dedicate this work to the memory of Dr. Ricardo Renzo Brentani, a mentor and exceptional scientist.

* This work was supported by CIHR (Canada, CIHR # MOP 93651 MAMP and CIHR #MOP-84260 to GD), PrioNet-Canada (MAMP, VFP and VRM), FAPESP (VRM, MAMP) and CAPES (VRM). I.S. and F.A.C. received fellowships from CNPq (Brazil). F.B. received a fellowship from DFAIT-Canada. G.D. is a CIHR New Investigator and Senior Scientist of the Beatrice Hunter Cancer Research Institute.

S This article contains supplemental Fig. S1.

[e] To whom correspondence should be addressed: mprado@robarts.ca, Tel: 1 519-9315777 Ext. 24888; vprado@robarts.ca, Tel: 1 519 9315777 Ext. 24889; vmartins@cipe.accamargo.org.br, Tel: 55 11 2189 5000 Ext. 2973.

[f] These authors contributed equally to this work.

REFERENCES

1. Picard, D. (2002) Heat-shock protein 90, a chaperone for folding and regulation. *Cell Mol. Life Sci.* **59,** 1640–1648
2. Chen, S., Prapapanich, V., Rimerman, R. A., Honoré, B., and Smith, D. F. (1996) Interactions of p60, a mediator of progesterone receptor assembly, with heat shock proteins hsp90 and hsp70. *Mol. Endocrinol.* **10,** 682–693
3. Chen, S., and Smith, D. F. (1998) Hop as an adaptor in the heat shock protein 70 (Hsp70) and hsp90 chaperone machinery. *J. Biol. Chem.* **273,** 35194–35200
4. Taipale, M., Jarosz, D. F., and Lindquist, S. (2010) HSP90 at the hub of protein homeostasis: emerging mechanistic insights. *Nat. Rev. Mol. Cell Biol.* **11,** 515–528
5. Schmid, A. B., Lagleder, S., Grawert, M. A., Rohl, A., Hagn, F., Wandinger, S. K., Cox, M. B., Demmer, O., Richter, K., Groll, M., Kessler, H., and Buchner, J. (2012) The architecture of functional modules in the Hsp90 co-chaperone Sti1/Hop. *EMBO J.* **31,** 1506–1517.
6. Prodromou, C., Siligardi, G., O'Brien, R., Woolfson, D. N., Regan, L., Panaretou, B., Ladbury, J. E., Piper, P. W., and Pearl, L. H. (1999) Regulation of Hsp90 ATPase activity by tetratricopeptide repeat (TPR)-domain co-chaperones. *EMBO J.* **18,** 754–762
7. Richter, K., Muschler, P., Hainzl, O., Reinstein, J., and Buchner, J. (2003) Sti1 is a non-competitive inhibitor of the Hsp90 ATPase. Binding prevents the N-terminal dimerization reaction during the atpase cycle. *J. Biol. Chem.* **278,** 10328–10333
8. Tsai, C. L., Tsai, C. N., Lin, C. Y., Chen, H. W., Lee, Y. S., Chao, A., Wang, T. H., Wang, H. S., and Lai, C. H. (2012) Secreted Stress-Induced Phosphoprotein 1 Activates the ALK2-SMAD Signaling Pathways and Promotes Cell Proliferation of Ovarian Cancer Cells. *Cell Rep.* **2,** 283–293.
9. Wang, T. H., Chao, A., Tsai, C. L., Chang, C. L., Chen, S. H., Lee, Y. S., Chen, J. K., Lin, Y. J., Chang, P. Y., Wang, C. J., Chao, A. S., Chang, S. D., Chang, T. C., Lai, C. H., and Wang, H. S. (2010) Stress-induced phosphoprotein 1 as a secreted biomarker for human ovarian cancer promotes cancer cell proliferation. *Mol. Cell. Proteomics.* **9,** 1873–1884
10. Arantes, C., Nomizo, R., Lopes, M. H., Hajj, G. N., Lima, F. R., and Martins, V. R. (2009) Prion protein and its ligand stress inducible protein 1 regulate astrocyte development. *Glia* **57,** 1439–1449
11. Hajj, G. N., Arantes, C. P., Dias, M. V., Roffe, M., Costa-Silva, B., Lopes, M. H., Porto-Carreiro, I., Rabachini, T., Lima, F. R., Beraldo, F. H., Prado, M. M., Linden, R., and Martins, V. R. (2013) The unconventional secretion of stress-inducible protein 1 by a heterogeneous population of extracellular vesicles. *Cell Mol. Life Sci.* **70,** 3211–3227.
12. Lima, F. R., Arantes, C. P., Muras, A. G., Nomizo, R., Brentani, R. R., and Martins, V. R. (2007) Cellular prion protein expression in astrocytes modulates neuronal survival and differentiation. *J. Neurochem.* **103,** 2164–2176
13. Caetano, F. A., Lopes, M. H., Hajj, G. N., Machado, C. F., Pinto, A. C., Magalhães, A. C., Vieira, M. P., Américo, T. A., Massensini, A. R., Priola, S. A., Vorberg, I., Gomez, M. V., Linden, R., Prado, V. F., Martins, V. R., and Prado, M. A. (2008) Endocytosis of prion protein is required for ERK1/2 signaling induced by stress-inducible protein 1. *J. Neurosci.* **28,** 6691–6702
14. Beraldo, F. H., Arantes, C. P., Santos, T. G., Queiroz, N. G., Young, K., Rylett, R. J., Markus, R. P., Prado, M. A., and Martins, V. R. (2010) Role of alpha7 nicotinic acetylcholine receptor in calcium signaling induced by prion protein interaction with stress-inducible protein 1. *J. Biol. Chem.* **285,** 36542–36550
15. Chiarini, L. B., Freitas, A. R., Zanata, S. M., Brentani, R. R., Martins, V. R., and Linden, R. (2002) Cellular prion protein transduces neuroprotective signals. *EMBO J.* **21,** 3317–3326
16. Lopes, M. H., Hajj, G. N., Muras, A. G., Mancini, G. L., Castro, R. M., Ribeiro, K. C., Brentani, R. R., Linden, R., and Martins, V. R. (2005) Interaction of cellular prion and stress-inducible protein 1 promotes neuritogenesis and neuroprotection by distinct signaling pathways. *J. Neurosci.* **25,** 11330–11339
17. Roffé, M., Beraldo, F. H., Bester, R., Nunziante, M., Bach, C., Mancini, G., Gilch, S., Vorberg, I., Castilho, B. A., Martins, V. R., and Hajj, G. N. (2010) Prion protein interaction with stress-inducible protein 1 enhances neuronal protein synthesis via mTOR. *Proc. Natl. Acad. Sci. U.S.A.* **107,** 13147–13152
18. Zanata, S. M., Lopes, M. H., Mercadante, A. F., Hajj, G. N., Chiarini, L. B., Nomizo, R., Freitas, A. R., Cabral, A. L., Lee, K. S., Juliano, M. A., de, Oliveira, E., Jachieri, S. G., Burlingame, A., Huang, L., Linden, R., Brentani, R. R., and Martins, V. R. (2002) Stress-inducible protein 1 is a cell surface ligand for cellular prion that triggers neuroprotection. *EMBO J.* **21,** 3307–3316
19. Chang, H. C., Nathan, D. F., and Lindquist, S. (1997) In vivo analysis of the Hsp90 cochaperone Sti1 (p60). *Mol. Cell. Biol.* **17,** 318–325
20. Song, H. O., Lee, W., An, K., Lee, H. S., Cho, J. H., Park, Z. Y., and Ahnn, J. (2009) C. elegans STI-1, the homolog of Sti1/Hop, is involved in aging and stress response. *J. Mol. Biol.* **390,** 604–617
21. Beraldo, F. H., Soares, I. N., Goncalves, D. F., Fan, J., Thomas, A. A., Santos, T. G., Mohammad, A. H., Roffe, M., Calder, M. D., Nikolova, S., Hajj, G. N., Guimaraes, A. L., Massensini, A. R., Welch, I., Betts, D. H., Gros, R., Drangova, M., Watson, A. J., Bartha, R., Prado, V. F., Martins, V. R., and Prado, M. A. (2013) Stress-inducible phosphoprotein 1 has unique co-chaperone activity during development and regulates cellular response to ischemia via prion protein. *FASEB J.* **27,** 3594–3607.
22. Honoré, B., Leffers, H., Madsen, P., Rasmussen, H. H., Vandekerckhove, J., and Celis, J. E. (1992) Molecular cloning and expression of a trans-

formation-sensitive human protein containing the TPR motif and sharing identity to the stress-inducible yeast protein STI1. *J. Biol. Chem.* **267,** 8485–8491
23. Longshaw, V. M., Chapple, J. P., Balda, M. S., Cheetham, M. E., and Blatch, G. L. (2004) Nuclear translocation of the Hsp70/Hsp90 organizing protein mSTI1 is regulated by cell cycle kinases. *J. Cell Sci.* **117,** 701–710
24. Daniel, S., Bradley, G., Longshaw, V. M., Söti, C., Csermely, P., and Blatch, G. L. (2008) Nuclear translocation of the phosphoprotein Hop (Hsp70/Hsp90 organizing protein) occurs under heat shock, and its proposed nuclear localization signal is involved in Hsp90 binding. *Biochim. Biophys. Acta* **1783,** 1003–1014
25. Bredemeyer, A. J., Carrigan, P. E., Fehniger, T. A., Smith, D. F., and Ley, T. J. (2006) Hop cleavage and function in granzyme B-induced apoptosis. *J. Biol. Chem.* **281,** 37130–37141
26. Schneider, L., Fumagalli, M., and d'Adda, di, Fagagna, F. (2012) Terminally differentiated astrocytes lack DNA damage response signaling and are radioresistant but retain DNA repair proficiency. *Cell Death. Differ.* **19,** 582–591
27. Guzman, M. S., De, Jaeger, X., Raulic, S., Souza, I. A., Li, A. X., Schmid, S., Menon, R. S., Gainetdinov, R. R., Caron, M. G., Bartha, R., Prado, V. F., and Prado, M. A. (2011) Elimination of the vesicular acetylcholine transporter in the striatum reveals regulation of behaviour by cholinergic-glutamatergic co-transmission. *PLoS Biol.* **9,** e1001194
28. Zanata, S. M., Lopes, M. H., Mercadante, A. F., Hajj, G. N., Chiarini, L. B., Nomizo, R., Freitas, A. R., Cabral, A. L., Lee, K. S., Juliano, M. A., de Oliveira, E., Jachieri, S. G., Burlingame, A., Huang, L., Linden, R., Brentani, R. R., and Martins, V. R. (2002) Stress-inducible protein 1 is a cell surface ligand for cellular prion that triggers neuroprotection. *EMBO J.* **21,** 3307–3316
29. Ferreira, L. T., Santos, M. S., Kolmakova, N. G., Koenen, J., Barbosa, J., Jr., Gomez, M. V., Guatimosim, C., Zhang, X., Parsons, S. M., Prado, V. F., and Prado, M. A. (2005) Structural requirements for steady-state localization of the vesicular acetylcholine transporter. *J. Neurochem.* **94,** 957–969
30. Fischer, M. J. (2010) Amine coupling through EDC/NHS: a practical approach. *Methods Mol. Biol.* **627,** 55–73
31. Lukas, J., Lukas, C., and Bartek, J. (2011) More than just a focus: The chromatin response to DNA damage and its role in genome integrity maintenance. *Nat. Cell Biol.* **13,** 1161–1169
32. Nacerddine, K., Lehembre, F., Bhaumik, M., Artus, J., Cohen-Tannoudji, M., Babinet, C., Pandolfi, P. P., and Dejean, A. (2005) The SUMO pathway is essential for nuclear integrity and chromosome segregation in mice. *Dev. Cell* **9,** 769–779
33. Palvimo, J. J. (2007) PIAS proteins as regulators of small ubiquitin-related modifier (SUMO) modifications and transcription. *Biochem. Soc. Trans.* **35,** 1405–1408
34. Rytinki, M. M., Kaikkonen, S., Pehkonen, P., Jääskelainen, T., and Palvimo, J. J. (2009) PIAS proteins: pleiotropic interactors associated with SUMO. *Cell Mol. Life Sci.* **66,** 3029–3041
35. Wotton, D., and Merrill, J. C. (2007) Pc2 and SUMOylation. *Biochem. Soc. Trans.* **35,** 1401–1404
36. Lopes, M. H., Hajj, G. N., Muras, A. G., Mancini, G. L., Castro, R. M., Ribeiro, K. C., Brentani, R. R., Linden, R., and Martins, V. R. (2005) Interaction of cellular prion and stress-inducible protein 1 promotes neuritogenesis and neuroprotection by distinct signaling pathways. *J. Neurosci.* **25,** 11330–11339
37. Eskiw, C. H., Dellaire, G., Mymryk, J. S., and Bazett-Jones, D. P. (2003) Size, position and dynamic behavior of PML nuclear bodies following cell stress as a paradigm for supramolecular trafficking and assembly. *J. Cell Sci.* **116,** 4455–4466
38. Dellaire, G., and Bazett-Jones, D. P. (2004) PML nuclear bodies: dynamic sensors of DNA damage and cellular stress. *Bioessays* **26,** 963–977
39. Ching, R. W., Dellaire, G., Eskiw, C. H., and Bazett-Jones, D. P. (2005) PML bodies: a meeting place for genomic loci? *J. Cell Sci.* **118,** 847–854
40. Lallemand-Breitenbach, V., and de, Thé, H. (2010) PML nuclear bodies. *Cold Spring Harb. Perspect. Biol.* **2,** a000661
41. Geiss-Friedlander, R., and Melchior, F. (2007) Concepts in sumoylation: a decade on. *Nat. Rev. Mol. Cell Biol.* **8,** 947–956
42. Dohmen, R. J. (2004) SUMO protein modification. *Biochim. Biophys. Acta* **1695,** 113–131
43. Heun, P. (2007) SUMOrganization of the nucleus. *Curr. Opin. Cell Biol.* **19,** 350–355
44. Galisson, F., Mahrouche, L., Courcelles, M., Bonneil, E., Meloche, S., Chelbi-Alix, M. K., and Thibault, P. (2011) A novel proteomics approach to identify SUMOylated proteins and their modification sites in human cells. *Mol. Cell Proteomics.* **10,** M110
45. Squatrito, M., Brennan, C. W., Helmy, K., Huse, J. T., Petrini, J. H., and Holland, E. C. (2010) Loss of ATM/Chk2/p53 pathway components accelerates tumor development and contributes to radiation resistance in gliomas. *Cancer Cell* **18,** 619–629
46. Jones, T. S., and Holland, E. C. (2012) Standard of care therapy for malignant glioma and its effect on tumor and stromal cells. *Oncogene* **31,** 1995–2006
47. Mabb, A. M., Wuerzberger-Davis, S. M., and Miyamoto, S. (2006) PIASy mediates NEMO sumoylation and NF-kappaB activation in response to genotoxic stress. *Nat. Cell Biol.* **8,** 986–993
48. Galanty, Y., Belotserkovskaya, R., Coates, J., Polo, S., Miller, K. M., and Jackson, S. P. (2009) Mammalian SUMO E3-ligases PIAS1 and PIAS4 promote responses to DNA double-strand breaks. *Nature* **462,** 935–939
49. Rabellino, A., Carter, B. J., Konstantinidou, G., Shwu-Yuan, W., Rimessi, A., Byers, L. A., Heymach, J. V., Girard, L., Chiang, C. M., Teruya-Feldstein, J., and Scaglioni, P. P. (2012) The SUMO E3-ligase PIAS1 regulates the tumor suppressor PML and its oncogenic counterpart PML-RARA. *Cancer Res.* **72,** 2275–2284.
50. Arlander, S. J., Felts, S. J., Wagner, J. M., Stensgard, B., Toft, D. O., and Karnitz, L. M. (2006) Chaperoning checkpoint kinase 1 (Chk1), an Hsp90 client, with purified chaperones. *J. Biol. Chem.* **281,** 2989–2998
51. Flom, G., Weekes, J., and Johnson, J. L. (2005) Novel interaction of the Hsp90 chaperone machine with Ssl2, an essential DNA helicase in Saccharomyces cerevisiae. *Curr. Genet.* **47,** 368–380
52. Boichuk, S., Hu, L., Makielski, K., Pandolfi, P. P., and Gjoerup, O. V. (2011) Functional connection between Rad51 and PML in homology-directed repair. *PLoS ONE* **6,** e25814
53. Bernardi, R., and Pandolfi, P. P. (2007) Structure, dynamics and functions of promyelocytic leukaemia nuclear bodies. *Nat. Rev. Mol. Cell Biol.* **8,** 1006–1016
54. Gostissa, M., Hofmann, T. G., Will, H., and Del, Sal, G. (2003) Regulation of p53 functions: let's meet at the nuclear bodies. *Curr. Opin. Cell Biol.* **15,** 351–357
55. Renner, F., Moreno, R., and Schmitz, M. L. (2010) SUMOylation-dependent localization of IKKepsilon in PML nuclear bodies is essential for protection against DNA-damage-triggered cell death. *Mol. Cell* **37,** 503–515
56. Carbone, R., Pearson, M., Minucci, S., and Pelicci, P. G. (2002) PML NBs associate with the hMre11 complex and p53 at sites of irradiation induced DNA damage. *Oncogene* **21,** 1633–1640
57. Quanz, M., Herbette, A., Sayarath, M., de, Koning, L., Dubois, T., Sun, J. S., and Dutreix, M. (2012) Heat shock protein 90alpha (Hsp90alpha) is phosphorylated in response to DNA damage and accumulates in repair foci. *J. Biol. Chem.* **287,** 8803–8815
58. Stecklein, S. R., Kumaraswamy, E., Behbod, F., Wang, W., Chaguturu, V., Harlan-Williams, L. M., and Jensen, R. A. (2012) BRCA1 and HSP90 cooperate in homologous and non-homologous DNA double-strand-break repair and G2/M checkpoint activation. *Proc. Natl. Acad. Sci. U.S.A.* **109,** 13650–13655
59. Dunn, G. P., Rinne, M. L., Wykosky, J., Genovese, G., Quayle, S. N., Dunn, I. F., Agarwalla, P. K., Chheda, M. G., Campos, B., Wang, A., Brennan, C., Ligon, K. L., Furnari, F., Cavenee, W. K., Depinho, R. A., Chin, L., and Hahn, W. C. (2012) Emerging insights into the molecular and cellular basis of glioblastoma. *Genes Dev.* **26,** 756–784
60. Tanaka, S., Louis, D. N., Curry, W. T., Batchelor, T. T., and Dietrich, J. (2013) Diagnostic and therapeutic avenues for glioblastoma: no longer a dead end? *Nat. Rev. Clin. Oncol.* **10,** 14–26
61. Iwanami, A., Gini, B., Zanca, C., Matsutani, T., Assuncao, A., Nael, A., Dang, J., Yang, H., Zhu, S., Kohyama, J., Kitabayashi, I., Cavenee, W. K., Cloughesy, T. F., Furnari, F. B., Nakamura, M., Toyama, Y., Okano, H., and Mischel, P. S. (2013) PML mediates glioblastoma resistance to mammalian target of rapamycin (mTOR)-targeted therapies. *Proc. Natl. Acad. Sci. U.S.A.*
62. Lallemand-Breitenbach, V., Zhu, J., Puvion, F., Koken, M., Honoré, N., Doubeikovsky, A., Duprez, E., Pandolfi, P. P., Puvion, E., Freemont, P., and de, Thé, H. (2001) Role of promyelocytic leukemia (PML) sumolation in nuclear body formation, 11S proteasome recruitment, and As2O3-

induced PML or PML/retinoic acid receptor alpha degradation. *J. Exp. Med.* **193,** 1361–1371
63. Lång, E., Grudic, A., Pankiv, S., Bruserud, O., Simonsen, A., Bjerkvig, R., Bjørås, M., and Bøe, S. O. (2012) The arsenic-based cure of acute promyelocytic leukemia promotes cytoplasmic sequestration of PML and PML/RARA through inhibition of PML body recycling. *Blood* **120,** 847–857
64. Reidy, M., and Masison, D. C. (2010) Sti1 regulation of Hsp70 and Hsp90 is critical for curing of Saccharomyces cerevisiae [PSI+] prions by Hsp104. *Mol. Cell. Biol.* **30,** 3542–3552
65. Horibe, T., Torisawa, A., Kohno, M., and Kawakami, K. (2012) Molecular mechanism of cytotoxicity induced by Hsp90-targeted Antp-TPR hybrid peptide in glioblastoma cells. *Mol. Cancer* **11,** 59
66. Gangaraju, V. K., Yin, H., Weiner, M. M., Wang, J., Huang, X. A., and Lin, H. (2011) Drosophila Piwi functions in Hsp90-mediated suppression of phenotypic variation. *Nat. Genet.* **43,** 153–158